

Optimization meets Machine Learning: An Exact Algorithm for Semi-Supervised Support Vector Machines

Veronica Piccialli^{1*}, Jan Schwiddessen² and Antonio M. Sudoso¹

^{1*}Department of Computer, Control and Management Engineering,
Sapienza University of Rome, Via Ariosto 25, Rome, 00185, Italy.

²Institut für Mathematik, Alpen-Adria-Universität Klagenfurt,
Universitätstraße 65-67, Klagenfurt, 9020, Austria.

*Corresponding author(s). E-mail(s): veronica.piccialli@uniroma1.it;
Contributing authors: jan.schwiddessen@aau.at;
antoniomaria.sudoso@uniroma1.it;

Abstract

Support vector machines (SVMs) are well-studied supervised learning models for binary classification. Large amounts of samples can be cheaply and easily obtained in many applications. What is often a costly and error-prone process is to label these data points manually. Semi-supervised support vector machines (S3VMs) extend the well-known SVM classifiers to the semi-supervised approach, aiming to maximize the margin between samples in the presence of unlabeled data. By leveraging both labeled and unlabeled data, S3VMs attempt to achieve better accuracy and robustness than traditional SVMs. Unfortunately, the resulting optimization problem is non-convex and hence difficult to solve exactly. This paper presents a new branch-and-cut approach for S3VMs using semidefinite programming (SDP) relaxations. We apply optimality-based bound tightening to bound the feasible set. Box constraints allow us to include valid inequalities, strengthening the lower bound. The resulting SDP relaxation provides bounds that are significantly stronger than the ones available in the literature. For the upper bound, instead, we define a local search heuristic exploiting the solution of the SDP relaxation. Computational results highlight the algorithm's efficiency, showing its capability to solve instances with ten times more data points than the ones solved in the literature.

Keywords: Global Optimization, SVM, Branch-and-Cut, Semidefinite Programming

1 Introduction

Support Vector Machines (SVMs) are a powerful class of supervised machine learning algorithms used for classification and regression tasks [1]. SVMs are particularly effective in handling high-dimensional data and can be applied to both linearly separable and non-linearly separable datasets. The main idea behind SVMs is to find an optimal hyperplane that maximally separates the data points belonging to different classes in a feature space. This hyperplane is selected so that the margin, which is the distance between the hyperplane and the nearest data points from each class (called support vectors), is maximized. By maximizing the margin, SVMs aim to achieve better generalization and improve the ability to classify unseen data accurately. The SVM training problem can be equivalently formulated as a quadratic convex problem with linear constraints or, by Wolfe’s duality theory, as a quadratic convex problem with one linear constraint and box constraints. Depending on the formulation, several optimization algorithms have been designed specifically for SVM training. We refer the reader to the survey [2] for an overview of the essential optimization methods for training SVMs.

Semi-supervised Support Vector Machines (S3VMs) are an extension of the traditional (supervised) SVMs that incorporate both labeled and unlabeled data during the training process [3]. Obtaining labeled data can be costly and time-consuming in many real-world applications, whereas unlabeled data are relatively easy to obtain in large quantities. When only a small percentage of the collected samples is labeled, learning a classification function is very likely to produce an inconsistent model, which would not be reliable for classifying future data. The motivation behind S3VMs is to exploit the unlabeled data to learn a decision boundary that is more robust and generalizable. In fact, by maximizing the margin in the presence of unlabeled data, the decision boundary produced by S3VMs traverses through low data-density regions while adhering to the labeled data points in the input space. In other words, this approach applies the cluster assumption to semi-supervised learning, which states that data points belonging to the same cluster have the same labels [4, 5].

The design of SVMs with partially labeled datasets has been a highly active area of research. Much of this work revolves around a key concept: solving the conventional SVM problem while considering the unknown labels as extra optimization variables. However, the improved performance of S3VMs is obtained at the sacrifice of computational complexity. While the underlying optimization problem of SVMs is convex, this is not the case for S3VMs, where the problem becomes non-convex and has many low-quality solutions [6]. Since its introduction in [3], a wide range of techniques has been employed to find good-quality solutions to the non-convex optimization problem associated with S3VMs [7]. These techniques include combinatorial search [8, 9], gradient descent [4], continuation techniques [10], convex-concave procedures [11, 12], semidefinite programming [13, 14], nonsmooth optimization [15], and deterministic

annealing [16]. See the work by Chapelle et al. [6] and references therein for an overview of optimization procedures for S3VMs.

Many studies have demonstrated that S3VM implementations exhibit varying levels of empirical success. As shown in [17], this discrepancy is closely linked to their vulnerability to issues related to local optimizers. Empirical results on some semi-supervised tasks presented in [17] show that the exact solution found by the branch-and-bound method has excellent generalization performance. In contrast, other S3VM implementations based on local optimization methods perform poorly. Local algorithms are designed to find solutions within a local region, and they can get trapped in low-quality local optima when dealing with non-convex problems. In the case of S3VMs, this can lead to a suboptimal hyperplane that does not generalize well to unseen data. Similar to most semi-supervised learning methods, there is no guarantee that S3VMs will outperform their supervised counterparts. This uncertainty stems from two potential scenarios: (a) the cluster assumption may not hold, and (b) the cluster assumption holds, but the presence of several local minima is problematic.

Chapelle et al. [6] conducted an empirical investigation comparing different S3VM implementations with a global optimizer. Their findings suggested that performance degradation is primarily due to suboptimal local minima, establishing a clear correlation between generalization performance and the S3VM objective function. Consequently, when the cluster assumption holds and hyperparameters are appropriately chosen, minimizing the S3VM objective is expected to be a suitable approach. However, due to the non-convex nature of the problem, minimizing the S3VM objective is not a straightforward task, requiring the application of diverse optimization techniques, each with varying degrees of success. Moreover, the study by Chapelle et al. [6] revealed that no single heuristic method consistently outperforms others regarding generalization performance. This underscores the ongoing need for improved global optimization methods to optimize the S3VM objective function. Our paper addresses this gap by proposing an exact algorithm based on the branch-and-cut technique to achieve globally optimal solutions for S3VMs.

2 Related Work

This section reviews the exact approaches proposed in the literature to tackle S3VMs. Due to the complexity of the associated optimization problem, the computational time required for solving S3VM instances to global optimality quickly increases as the number of data points grows. This is why applications of S3VMs have been restricted to small-size problems. Most exact approaches in the literature are based on the branch-and-bound technique. A first branch-and-bound algorithm is proposed by Bennett and Demiriz [3]. The authors show that the L1-norm linear S3VM model can be reformulated as a Mixed-Integer Program (MIP) and solved exactly using integer programming tools. Instead, Chapelle et al. [17] propose a branch-and-bound algorithm for L2-norm S3VMs. This algorithm performs a search over all possible labels and prunes large parts of the solution space based on lower bounds on the optimal S3VM objective. For the lower bound, they use the objective value of a standard SVM trained on the associated labeled set. Next, they produce a binary enumeration tree where nodes are

associated with a fixed partial labeling of the unlabeled dataset, and the two children correspond to the labeling of some new unlabeled data point. The root corresponds to the initial set of labeled examples, and the leaves correspond to a complete labeling of the data. Moving down in the tree, a labeling-confidence criterion is used to choose an unlabeled example on which to branch. The overall algorithm is able to return a globally optimal solution in a reasonable amount of time only for small-scale instances (less than 50 data points). Other approaches for solving S3VMs have been put forward. For instance, several studies have proposed convex relaxations of the objective function, which can be solved using Quadratic Programming (QP) and Semidefinite Programming (SDP) tools [14, 18, 19]. A semidefinite programming problem involves optimizing a linear objective function over the intersection of the cone of positive semidefinite matrices with an affine subspace. SDPs are convex optimization problems, and all well-posed SDPs can be solved in polynomial time, typically using interior-point methods. SDP relaxations are known to provide strong dual bounds for challenging combinatorial optimization problems. For a comprehensive overview of the theory, algorithms, and applications of semidefinite programming, we recommend referring to [20].

More recently, Tian and Luo [21] have proposed a new branch-and-bound algorithm for the L2-norm S3VM. First, they transform the original problem into a non-convex quadratically constrained quadratic programming (QCQP) problem. Then, to provide computationally efficient lower bounds, they apply Lagrangian relaxation to the QCQP model and dualize the non-convex quadratic constraints. The Lagrange multipliers are estimated by solving an auxiliary SDP and are then propagated downward to the child nodes during every branching step. At its core, the algorithm is a heuristic inspired by the branch-and-bound technique, involving a maximum number of branching decisions (labelings). For small problems, this decision count is fixed at 30, while for larger instances, the algorithm terminates the enumeration process when 50% of unlabeled points have been labeled. It is worth highlighting that, in the general setting, this algorithm falls short of providing a certificate of global optimality. To the best of our knowledge, this is the most recent method based on the branch-and-bound technique available in the literature for L2-norm S3VMs.

In this paper, we present a novel exact algorithm based on the branch-and-cut technique. We enhance an existing SDP relaxation by employing sophisticated techniques from the global optimization literature. Specifically tailored to our problem, these methods yield significantly stronger bounds compared to those reported in existing literature. More in detail, the main original contributions of this paper are:

1. We propose the first SDP-based branch-and-cut algorithm producing globally optimal solutions for S3VM. We perform bound tightening to derive optimality-based box constraints that allow us to strengthen the basic SDP relaxation available in the literature. We solve the resulting SDP relaxation through a cutting-plane procedure. We define an effective local search heuristic that exploits the solution of the SDP relaxation.
2. We prove the tightness of the SDP relaxation for an ideal kernel function such that the S3VM objective function aligns with the ground truth.

3. We perform an extensive set of numerical experiments on both synthetic and real-world instances. Our findings illustrate the algorithm’s consistent ability to yield small optimality gaps for large-scale instances (up to 569 data points), a problem size approximately ten times larger than those addressed by existing exact algorithms in the literature.
4. We thoroughly analyze our results from both the mathematical optimization and machine learning perspectives, highlighting the advantages of using an exact algorithm.

The remainder of this paper is organized as follows. In Section 3, we present the S3VM formulation and the convex relaxations available in the literature. Section 4 illustrates the ingredients of the proposed branch-and-cut approach, namely the SDP relaxation, the primal heuristic, and the branching strategy. In Section 5, we prove the tightness of the SDP relaxation under the assumption of the ideal kernel matrix. Section 6 presents computational results on both synthetic and real-world instances. Finally, Section 7 concludes the paper with future research directions.

Notation

Let \mathbb{S}^n be the set of all $n \times n$ real symmetric matrices. We denote by $M \succeq 0$ a positive semidefinite matrix M and by \mathbb{S}_+^n the set of all positive semidefinite matrices of size $n \times n$. Analogously, we denote by $M \succ 0$ a positive definite matrix M and by \mathbb{S}_{++}^n the set of all positive definite matrices of size $n \times n$. We denote the trace inner product by $\langle \cdot, \cdot \rangle$. That is, for any $A, B \in \mathbb{R}^{n \times m}$, we define $\langle A, B \rangle := \text{tr}(B^\top A)$. Given a matrix $A \in \mathbb{R}^{n \times m}$, A_{ij} denotes the element of A in the i -th row and j -th column. For two vectors $a, b \in \mathbb{R}^n$, $a \circ b$ denotes the element-wise product between a and b . Finally, we denote by e_n the vector of all ones of size n and by I_n the identity matrix of size $n \times n$. We omit the subscript when the size is clear from the context.

3 Semi-supervised Support Vector Machines

In this section, we introduce the mathematical programming formulation behind S3VMs. We are given a binary classification dataset consisting of l labeled points $\{(x_i, y_i)\}_{i=1}^l$ and $n - l$ unlabeled points $\{x_i\}_{i=l+1}^n$, where $x_i \in \mathbb{R}^d$ and $y_i \in \{-1, +1\}$ for $i \in \{1, \dots, n\}$. Similar to traditional SVMs, the primary objective of S3VMs is to determine the parameters $(w, b) \in \mathbb{R}^d \times \mathbb{R}$ of a separating hyperplane $w^\top x_i + b = 0$. This hyperplane separates all the data points in the input space into two classes by maximizing the distance between two supporting hyperplanes, namely $w^\top x_i + b = 1$ and $w^\top x_i + b = -1$, while ensuring accurate classification. The objective function to be optimized depends on both the decision boundary parameters (w, b) and the unknown labels $\{y_i\}_{i=l+1}^n$:

$$f(w, b, \{y_i\}_{i=l+1}^n) = \frac{1}{2} \|w\|_2^2 + C_l \sum_{i=1}^l H(y_i, o_i) + C_u \sum_{i=l+1}^n H(y_i, o_i), \quad (1)$$

where $o_i = w^\top x_i + b$ and H is a loss function. The hyperparameters C_l and C_u are used to give more importance to the labeled and unlabeled error components, respectively. The Hinge loss, defined as

$$H(y_i, o_i) = \max(0, 1 - y_i o_i)^p,$$

is the most commonly used loss function and can be penalized either linearly ($p = 1$) or quadratically ($p = 2$). In the remainder of this paper, we will consider $p = 2$ which gives rise to the L2-norm S3VM formulation.

It is important to note that excluding the third term from (1) simplifies the formulation. From an optimization perspective, reducing the value of C_u makes the unlabeled loss function less non-convex. In particular, when $C_u = 0$, the objective function (1) reflects a conventional SVM training problem. Hence, the hyperparameter C_u allows for the control of the overall objective's non-convexity. Optimizing (1) results in a linear decision function, representing a separating hyperplane. Nonlinear boundaries can be achieved through the kernel trick [1, 2]. The recently developed optimization techniques for minimizing the S3VM objective can be broadly categorized into two groups: combinatorial and continuous approaches. Combinatorial approaches treat the labels $\{y_i\}_{i=l+1}^n$ of unlabeled data points as explicit optimization variables. In contrast, continuous approaches do not consider unknown labels as optimization variables but instead minimize modified versions of (1) using continuous optimization techniques [6]. Our methodology bridges aspects from both worlds, focusing on a continuous optimization formulation while leveraging its underlying combinatorial nature.

3.1 Problem formulation

Consider a binary classification problem with n data points where the first l data points are already labeled and the remaining data points $l + 1, \dots, n$ are unlabeled. We assume that all data points are centered around the origin so that the bias term b can be set to zero [22]. To handle datasets that are not linearly separable, we map all data points into a higher-dimensional space using a mapping function $\phi : \mathbb{R}^d \rightarrow \mathbb{R}^m$ and then separate them using a hyperplane in this expanded space. This gives rise to the kernel-based S3VMs model, which can be formulated as the following MIP:

$$\begin{aligned} \min_{w, \xi, y^u} \quad & \frac{1}{2} \|w\|_2^2 + C_l \sum_{i=1}^l \xi_i^2 + C_u \sum_{i=l+1}^n \xi_i^2 \\ \text{s. t.} \quad & y_i w^\top \phi(x_i) \geq 1 - \xi_i, \quad i = 1, \dots, n, \\ & y^u := (y_{l+1}, \dots, y_n)^\top \in \{-1, +1\}^{n-l}, \end{aligned} \tag{2}$$

where we use the L2-norm penalization for misclassification errors ξ_i . For a given set of labels y^u , we consider the convex problem for building the SVM as

$$\begin{aligned} \min_{w, \xi} \quad & \frac{1}{2} \|w\|_2^2 + C_l \sum_{i=1}^l \xi_i^2 + C_u \sum_{i=l+1}^n \xi_i^2 \\ \text{s. t.} \quad & y_i w^\top \phi(x_i) \geq 1 - \xi_i, \quad i = 1, \dots, n. \end{aligned} \quad (3)$$

Since the mapping ϕ cannot be handled explicitly, a kernel function defined by $k(x_i, x_j) := \phi(x_i)^\top \phi(x_j)$, which computes the inner product of the input vectors in a higher-dimensional space, is used instead. Let $\alpha \in \mathbb{R}^n$ be the vector of dual multipliers associated with the primal constraints. Moreover, let \bar{K} be the kernel matrix, i.e., a symmetric and positive semidefinite matrix whose elements are computed by applying the kernel function to all pairs of input vectors, and let D be a diagonal matrix with $D_{ii} = \frac{1}{2C_l}$ for $i = 1, \dots, l$ and $D_{ii} = \frac{1}{2C_u}$ for $i = l+1, \dots, n$. Then the Wolfe dual [2] of Problem (3) is

$$\begin{aligned} \max_{\alpha} \quad & e^\top \alpha - \frac{1}{2} \alpha^\top (K \circ yy^\top) \alpha \\ \text{s. t.} \quad & \alpha \geq 0, \end{aligned} \quad (4)$$

where $K := \bar{K} + D$ is a positive definite matrix.

By looking at the Karush-Kuhn-Tucker (KKT) conditions and denoting by $\mu \in \mathbb{R}^n$ the multipliers of the nonnegativity constraints $\alpha \geq 0$, we derive the closed-form expression

$$\alpha^\star = (K \circ yy^\top)^{-1} (e + \mu) \quad (5)$$

for the solution of the dual. Recall that complementarity conditions imply that

$$\alpha_i \mu_i = 0, \quad i = 1, \dots, n. \quad (6)$$

Combining (5) and (6) and exploiting that $(K \circ yy^\top)^{-1} = K^{-1} \circ yy^\top$ and that for any $x, y \in \mathbb{R}^n$, $Q \succ 0$, it holds $x^\top (Q \circ yy^\top) x = (x \circ y)^\top Q (x \circ y)$, we can rewrite Problem (4) as

$$\begin{aligned} \min_{\mu} \quad & \frac{1}{2} ((\mu + e) \circ y)^\top K^{-1} ((\mu + e) \circ y) \\ \text{s. t.} \quad & \mu \geq 0. \end{aligned}$$

We then replace Problem (3) in Problem (2) and end up with the following MIP:

$$\begin{aligned} \min_{\mu, y^u} \quad & \frac{1}{2} ((\mu + e) \circ y)^\top K^{-1} ((\mu + e) \circ y) \\ \text{s. t.} \quad & \mu \geq 0, \quad y := (y^l; y^u)^\top, \quad y^u \in \{-1, 1\}^{n-l}. \end{aligned} \quad (7)$$

Now, if we set $v = (\mu + e) \circ y$, the (convex) objective function becomes $\frac{1}{2} v^\top K^{-1} v$. The constraints $\mu_i \geq 0$ become $y_i v_i \geq 1$ for labeled points and $v_i^2 \geq 1$ for unlabeled

points, yielding the following non-convex QCQP [14]:

$$\begin{aligned}
\min_v \quad & \frac{1}{2} v^\top K^{-1} v \\
\text{s. t.} \quad & y_i v_i \geq 1, \quad i = 1, \dots, l, \\
& v_i^2 \geq 1, \quad i = l+1, \dots, n, \\
& v \in \mathbb{R}^n.
\end{aligned} \tag{8}$$

Remark 1. *Given the complementarity condition (6), we have that whenever a data point x_i is a support vector, meaning $\alpha_i > 0$, it must hold that $\mu_i = 0$. Therefore, since $v_i = (\mu_i + 1)y_i$, we get $v_i = y_i$. However, this is only a necessary condition for x_i being a support vector since we may have $\alpha_i = \mu_i = 0$.*

From a feasible solution v of Problem (8), it is possible to obtain a feasible solution y of Problem (7) by setting $y_i = \text{sign}(v_i)$ for $i = 1, \dots, n$. Moreover, the objective function values of both problems coincide.

It is known that minimizing the S3VM objective does not necessarily align with the performance of the S3VM classifier in terms of accuracy. This discrepancy is primarily attributed to the presence of multiple local minima [6, 17]. However, even when Problem (8) is solved to global optimality, we empirically found that there is no guarantee that the resulting optimal S3VM classifier will exhibit high accuracy. Consequently, lower objective values do not consistently translate into improved classification performance. To address this issue, we introduce a balancing constraint to Problem (8). This constraint is also used to avoid trivial solutions (with all unlabeled data points being classified as belonging to a single class), especially when the number of labeled examples is significantly smaller than that of unlabeled ones [6]. To enhance the robustness of S3VM models, Chapelle and Zien [4] proposed modifications to the model in (2) by introducing a balancing constraint under the assumption of a linear kernel:

$$\frac{1}{(n-l)} \sum_{i=l+1}^n \text{sign}(w^\top x_i) = \frac{1}{l} \sum_{i=1}^l y_i. \tag{9}$$

This constraint ensures that the fraction of positive and negative assignments to the unlabeled data points also equals the fraction found in the labeled data points. For us, the equivalent of constraint (9) is:

$$\frac{1}{(n-l)} \sum_{i=l+1}^n \text{sign}(v_i) = \frac{1}{l} \sum_{i=1}^l y_i. \tag{10}$$

However, since this constraint cannot be handled explicitly, we decided to approximate it with the following new linear constraint:

$$\frac{1}{(n-l)} \sum_{i=l+1}^n v_i = \frac{1}{l} \sum_{i=1}^l y_i. \quad (11)$$

The above constraint is an approximation of (10). Its foundation lies in the connection between Problems (2) and (8), where the sign of v_i represents the decision for the i -th data point. Thanks to Remark 1, all support vectors satisfy $v_i = y_i$. Therefore, if all the points were support vectors, the two constraints (10) and (11) would coincide. However, we have $v_i = y_i(\mu_i + 1)$ for points that are not support vectors, which may result in $|v_i| > 1$. In this scenario, constraint (11) encourages a distribution of the signs of the v_i that mirrors the class distribution among the labeled data points.

While some approaches employing the S3VM formulation in (8) do not incorporate any class balancing constraint (see, e.g., [14, 21]), our specific focus is on solving the QCQP problem outlined in (8) while incorporating the balancing constraint (11). This adjustment is made to enhance the robustness and accuracy of the globally optimal solution, as reported in Section 6.5. Thus, our S3VM model becomes

$$\begin{aligned} \min_v \quad & \frac{1}{2} v^\top K^{-1} v \\ \text{s. t.} \quad & y_i v_i \geq 1, \quad i = 1, \dots, l, \\ & v_i^2 \geq 1, \quad i = l+1, \dots, n, \\ & \frac{1}{(n-l)} \sum_{i=l+1}^n v_i = \frac{1}{l} \sum_{i=1}^l y_i, \\ & v \in \mathbb{R}^n. \end{aligned} \quad (12)$$

From a practical standpoint, non-convex QCQP problems are one of the most challenging optimization problems: the current size of instances that can be solved to provable optimality by general-purpose solvers remains very small. Therefore, our aim is twofold: (i) relaxing the intractable program in (12) into a tractable conic program, yielding computationally efficient bounds; and (ii) developing a branch-and-cut algorithm capable of solving large-scale instances to global optimality.

3.2 Convex relaxations

In this section, we review the convex relaxations of Problem (8) proposed in the literature and introduce our starting relaxation. The literature explores two main alternatives: QP and SDP relaxations.

QP relaxations The standard QP relaxation is obtained by dropping the non-convex constraints $v_i^2 \geq 1$ for $i = l+1, \dots, n$ in Problem (8). Thus, lower bounds can be computed by solving the resulting convex QP. Alternatively, the authors in [21]

apply Lagrangian relaxation to Problem (8), penalizing violations of non-convex constraints in the objective function. The Lagrange multipliers are estimated by solving an auxiliary SDP. More in detail, for a fixed $\lambda \geq 0$, Problem (8) can be relaxed to the following problem:

$$\begin{aligned} \min_v \quad & \frac{1}{2} v^\top (K^{-1} - 2\text{Diag}(\lambda))v + e^\top \lambda \\ \text{s. t.} \quad & y_i v_i \geq 1, \quad i = 1, \dots, l \\ & v \in \mathbb{R}^n. \end{aligned} \tag{13}$$

The corresponding vector of Lagrange multipliers λ is estimated in [21] by solving the auxiliary SDP

$$\begin{aligned} \max_\lambda \quad & e^\top \lambda \\ \text{s. t.} \quad & K^{-1} - 2\text{Diag}(\lambda) \succeq 0, \\ & \lambda \geq 0. \end{aligned} \tag{14}$$

SDP relaxations Non-convex QCQPs can also be approximately solved via tractable SDP relaxations. Specifically, Problem (8) can be reformulated as the following non-convex SDP problem in a lifted space:

$$\begin{aligned} \min_{v, V} \quad & \frac{1}{2} \langle K^{-1}, V \rangle \\ \text{s. t.} \quad & y_i v_i \geq 1, \quad i = 1, \dots, l, \\ & \text{diag}(V) \geq e, \\ & V = vv^\top, \quad v \in \mathbb{R}^n. \end{aligned}$$

By relaxing the constraint $V = vv^\top$ into $V - vv^\top \succeq 0$ and applying the Schur complement, we end up with the basic SDP relaxation already considered in [14]:

$$\begin{aligned} \min_{\bar{V}} \quad & \frac{1}{2} \langle K^{-1}, V \rangle \\ \text{s. t.} \quad & y_i v_i \geq 1, \quad i = 1, \dots, l, \\ & \text{diag}(V) \geq e, \\ & \bar{V} = \begin{pmatrix} V & v \\ v^\top & 1 \end{pmatrix} \succeq 0, \quad v \in \mathbb{R}^n, \quad V \in \mathbb{S}^n. \end{aligned} \tag{15}$$

Problem (15) provides a lower bound on the optimal objective value of Problem (8). Clearly, the bound provided by Problem (15) is stronger than that provided by the QP relaxation. Tighter bounds can be obtained by solving the Doubly Nonnegative relaxation (DNN) of Problem (7). To this end, Bai and Yan [14] rewrite Problem (7) as a MIP using 0-1 variables. Then, they reformulate the problem as the following

non-convex QCQP:

$$\begin{aligned}
& \min_u \quad \frac{1}{2} u^\top \tilde{K}^{-1} u \\
& \text{s. t.} \quad y_i(2u_i - u_{i+n}) \geq 1, \quad i = 1, \dots, l, \\
& \quad u_j \geq 0, \quad u_{j+n} \geq 1, \quad u_j u_{j+n} - u_j^2 = 0, \quad j = 1, \dots, n, \\
& \quad u \in \mathbb{R}^{2n},
\end{aligned}$$

where $\tilde{K} := (4K^{-1}, -2K^{-1}; -2K^{-1}, K^{-1}) \in \mathbb{S}^{2n}$. By relaxing the constraint $U = uu^\top$ into $U - uu^\top \succeq 0$ and applying the Schur complement, the DNN relaxation reads

$$\begin{aligned}
& \min_{\bar{U}} \quad \frac{1}{2} \langle \bar{K}^{-1}, \bar{U} \rangle \\
& \text{s. t.} \quad y_i(2u_i - u_{i+n}) \geq 1, \quad i = 1, \dots, l, \\
& \quad U_{j,j+n} - U_{j,j} = 0, \quad u_{j+n} \geq 1, \quad j = 1, \dots, n, \\
& \quad U_{k,k} - u_k \geq 0, \quad k = 1, \dots, 2n, \\
& \quad \bar{U} = \begin{pmatrix} 1 & u^\top \\ u & U \end{pmatrix} \succeq 0, \quad \bar{U} \geq 0.
\end{aligned} \tag{16}$$

Although Problem (16) is a convex, its size is larger than that of the basic SDP (15). Specifically, Problem (16) involves optimizing a matrix variable of dimensions $(2n+1) \times (2n+1)$ over the intersection of the positive semidefinite cone and the nonnegative orthant. Moreover, according to our computational experiments, the DNN relaxation (16) provides a lower bound that is only slightly better than that of the basic SDP (15), and the computational effort to obtain such bound is much higher. Since existing SDP solvers struggle with large-size problems, the DNN relaxation (16) is not directly applicable within a branch-and-bound approach. This motivated us to strengthen the SDP relaxation (15) instead, leading to the derivation of a new relaxation and valid constraints. These enhancements provide high-quality and computationally efficient bounds when embedded into a branch-and-cut algorithm.

4 Branch-and-cut Approach

In this section, we present the main ingredients of our branch-and-cut algorithm. Specifically, we describe the lower bound computation, the primal heuristic, and the

branching scheme. We start by rewriting Problem (12) in the more convenient form

$$\begin{aligned}
\min_x \quad & x^\top C x \\
\text{s. t.} \quad & 1 = L_i \leq x_i, \quad i = 1, \dots, l : y_i = 1, \\
& x_i \leq U_i = -1, \quad i = 1, \dots, l : y_i = -1, \\
& x_i^2 \geq 1, \quad i = 1, \dots, n, \\
& \frac{1}{(n-l)} \sum_{i=l+1}^n x_i = \frac{1}{l} \sum_{i=1}^l y_i, \\
& x \in \mathbb{R}^n,
\end{aligned} \tag{17}$$

where $C = \frac{1}{2}K^{-1}$. In Problem (17), we have substituted the constraints $y_i x_i \geq 1$, $i = 1, \dots, l$, by writing them as explicit lower or upper bound constraints on the variables x_i . From now on, we focus on defining our branch-and-cut approach for solving Problem (17) to global optimality.

4.1 Lower bound computation

The success of any branch-and-cut algorithm relies on the quality and computational efficiency of its lower bounds. Strong lower bounds can significantly prune the search space, resulting in faster convergence and reduced computational effort. In the context of our problem, we utilize various global optimization tools to develop a sophisticated bounding routine, which is crucial for the overall efficiency of the algorithm. The first step is to introduce valid box constraints.

Bound tightening The feasible set of Problem (17) is unbounded. Nevertheless, it is possible to introduce optimality-based box constraints $L_i \leq x_i \leq U_i$ for all variables x_i once we have an upper bound on the optimal objective value of Problem (12). This is especially desirable for variables corresponding to unlabeled data points to derive further valid constraints later. The idea is to solve auxiliary convex optimization problems to compute lower and upper bounds on all the variables such that at least one globally optimal solution of Problem (12) remains within the restricted feasible set.

Given a non-convex optimization problem and a tractable convex relaxation of it, classical optimality-based bound tightening computes the tightest bounds valid for all relaxation solutions by in turn minimizing and maximizing each variable, and imposing an objective cutoff [23]. If UB denotes an upper bound for Problem (12), then we can compute a new lower bound L_i and a new upper bound U_i for variable x_i by solving

QCQPs of the form

$$\begin{aligned}
L_i/U_i = \min / \max \quad & x_i \\
\text{s. t.} \quad & L_i \leq x_i \leq U_i, \quad i = 1, \dots, n, \\
& x^\top C x \leq UB, \\
& \frac{1}{(n-l)} \sum_{i=l+1}^n x_i = \frac{1}{l} \sum_{i=1}^l y_i, \\
& x \in \mathbb{R}^n,
\end{aligned} \tag{18}$$

where some bound constraints are $-\infty$ or $+\infty$ in the beginning. With abuse of notation, we refer to L_i and U_i both as the initial bounds on the variables x_i in the feasible set definition and the updated bounds obtained from solving problems of type (18), with the new values replacing the old ones whenever a bound constraint is updated. Since C is a positive definite matrix, Problem (18) is a convex and can be solved efficiently. Applying a complete round of optimality-based bound tightening involves solving up to $2n$ convex QCQPs, each with one quadratic constraint. Note that the lower bound computation for variable x_i can be skipped if $L_i \geq 1$ already holds since the optimal objective value of (18) would most likely be L_i in this case. The same applies to the upper bound computation if $U_i \leq -1$ already holds.

Remark 2 (Projecting box constraints). *Whenever the optimal objective value of Problem (18) yields a new lower bound $L_i > -1$, we can set L_i to $L_i := \max\{L_i, 1\}$. This is due to the non-convex constraints $x_j^2 \geq 1$ in Problem (12) that require the absolute value of each variable to be at least one. Similarly, we can set U_i to $U_i := \min\{U_i, -1\}$ if the optimal objective value of Problem (18) yields an upper bound $U_i < 1$. In both cases, the label of the corresponding data point (-1 or $+1$) becomes fixed, and the non-convex constraint $x_i^2 \geq 1$ could be removed from Problem (12). This reduces the size of the branch-and-bound tree and significantly impacts the overall efficiency of the algorithm.*

Remark 2 gives a strong motivation to recompute the box constraints from time to time if new information is available. In fact, we solve all QCQPs of type (18) again whenever we have updated the best known upper bound UB .

Basic SDP relaxation Once lower and upper bounds on each variable have been computed by solving problems of type (18), Problem (17) can be equivalently stated

as the non-convex matrix optimization problem

$$\begin{aligned}
& \min_{x, X} \quad \langle C, X \rangle \\
& \text{s. t.} \quad L_i \leq x_i \leq U_i, \quad i = 1, \dots, n, \\
& \quad \quad 1 \leq X_{ii} \leq \max\{L_i^2, U_i^2\}, \quad i = 1, \dots, n \\
& \quad \quad \frac{1}{(n-l)} \sum_{i=l+1}^n x_i = \frac{1}{l} \sum_{i=1}^l y_i, \\
& \quad \quad X = xx^\top, \quad x \in \mathbb{R}^n.
\end{aligned} \tag{19}$$

In Problem (19), we have also bounded the main diagonal of X via the constraints $X_{ii} \leq \max\{L_i^2, U_i^2\}$ for $i = 1, \dots, n$. These can be derived by using the box constraints on x_i and the fact that $x_i^2 = X_{ii}$ must hold in any feasible solution of (19).

By relaxing the constraint $X = xx^\top$ into $X - xx^\top \succeq 0$ and applying the Schur complement, we end up with our first SDP relaxation

$$\begin{aligned}
& \min_{\bar{X}} \quad \langle C, X \rangle \\
& \text{s. t.} \quad L_i \leq x_i \leq U_i, \quad i = 1, \dots, n, \\
& \quad \quad 1 \leq X_{ii} \leq \max\{L_i^2, U_i^2\}, \quad i = 1, \dots, n, \\
& \quad \quad \frac{1}{(n-l)} \sum_{i=l+1}^n x_i = \frac{1}{l} \sum_{i=1}^l y_i, \\
& \quad \quad \bar{X} = \begin{pmatrix} X & x \\ x^\top & 1 \end{pmatrix} \succeq 0, \quad x \in \mathbb{R}^n, \quad X \in \mathbb{S}^n.
\end{aligned} \tag{20}$$

Proposition 1. *Assume that $L_i \in \mathbb{R}$ and $U_i \in \mathbb{R}$ are computed by solving problems of type (18) for $i = 1, \dots, n$. Then, Problem (20) provides a lower bound at least as strong as the one provided by Problem (15).*

Proof. The assumption on L_i and U_i implies that the box constraints $L_i \leq x_i \leq U_i$ are valid for Problem (17) for $i = 1, \dots, n$. Therefore, Problem (20) is a relaxation of Problem (12). The result then follows from the feasible set of Problem (20) being strictly contained in the feasible set of Problem (15). \square

Valid inequalities The SDP relaxation (20) can be strengthened by adding constraints that are also valid for any feasible solution of Problem (19). Since we have box constraints, the constraints coming from the Reformulation-Linearization Technique (RLT) [24] are an interesting class for us. They can be derived by multiplying the nonnegative expressions $x_i - L_i \geq 0$ and $U_i - x_i \geq 0$ by the nonnegative expressions $x_j - L_j \geq 0$ and $U_j - x_j \geq 0$ for all $i, j = 1, \dots, n$, $i < j$, and then expanding to

$$\begin{aligned}
X_{ij} & \geq \max\{U_i x_j + U_j x_i - U_i U_j, L_i x_j + L_j x_i - L_i L_j\}, \\
X_{ij} & \leq \min\{L_i x_j + U_j x_i - L_i U_j, U_i x_j + L_j x_i - U_i L_j\}.
\end{aligned} \tag{21}$$

It will become evident in the computational results in Section 6 that adding RLT inequalities (21) significantly improves the SDP relaxation (20). In the end, we obtain lower bounds for Problem (12) by solving the SDP

$$\begin{aligned}
& \min_{\bar{X}} \quad \langle C, X \rangle \\
& \text{s. t.} \quad L_i \leq x_i \leq U_i, \quad i = 1, \dots, n, \\
& \quad 1 \leq X_{ii} \leq \max\{L_i^2, U_i^2\}, \quad i = 1, \dots, n, \\
& \quad \frac{1}{(n-l)} \sum_{i=l+1}^n x_i = \frac{1}{l} \sum_{i=1}^l y_i, \\
& \quad X_{ij} \geq U_i x_j + U_j x_i - U_i U_j, \quad i, j = 1, \dots, n, \ i < j, \\
& \quad X_{ij} \geq L_i x_j + L_j x_i - L_i L_j, \quad i, j = 1, \dots, n, \ i < j, \\
& \quad X_{ij} \leq L_i x_j + U_j x_i - L_i U_j, \quad i, j = 1, \dots, n, \ i < j, \\
& \quad X_{ij} \leq U_i x_j + L_j x_i - U_i L_j, \quad i, j = 1, \dots, n, \ i < j. \\
& \quad \bar{X} = \begin{pmatrix} X & x \\ x^\top & 1 \end{pmatrix} \succeq 0, \ x \in \mathbb{R}^n, \ X \in \mathbb{S}^n.
\end{aligned} \tag{22}$$

Despite having only $\mathcal{O}(n^2)$ RLT inequalities, adding them all at once would make the relaxation intractable, even for a moderate number of data points, when using off-the-shelf interior-point solvers. Thus, we treat them as cutting planes and only add a few of the most violated ones during each cutting-plane iteration.

Further valid constraints for (19) can be generated by multiplying the balancing constraint (11) by any variable x_j , $j = 1, \dots, n$, resulting in the constraints

$$\frac{1}{(n-l)} \sum_{i=l+1}^n x_i x_j = \left(\frac{1}{l} \sum_{i=1}^l y_i \right) x_j, \quad j = 1, \dots, n.$$

These product constraints can then be linearized and added to the SDP relaxation (22) by replacing any quadratic term $x_i x_j$ by X_{ij} . Adding these constraints improves the lower bound but slows down computation. Therefore, they can be beneficial for problems with a weak lower bound, but otherwise, they can be neglected.

For several reasons, the box constraints $L_i \leq x_i \leq U_i$ play a crucial role in our setting. Firstly, they indicate whether the sign of a variable x_i is known, which is the case whenever $L_i \geq 1$ or $U_i \leq -1$ holds. This reduces the degree of non-convexity in the problem since the constraint $x_i^2 \geq 1$ can be removed. Secondly, tighter box constraints can significantly impact the quality of our lower bound as the RLT inequalities become more restrictive. The box constraints can be improved by resolving problems of type (18) whenever a better upper bound for (12) is found. Additionally, every branching step also impacts the box constraints, see Section 4.3.

Marginals-based bound tightening Moreover, to further tighten the box constraints, we use a standard technique in global optimization, namely marginals-based

bound tightening as proposed in [25]. The general idea is the following, see [25, Theorem 2]: let $g(x, X) \leq 0$ be an active constraint in our SDP relaxation (22) with corresponding dual multiplier $\lambda > 0$ at the optimal solution with objective value LB . Moreover, let UB be an upper bound on Problem (17). Then the constraint

$$g(x, X) \geq -\frac{UB - LB}{\lambda} \quad (23)$$

is valid for all solutions of Problem (17) with objective value better than UB . In other words, the constraint (23) may cut off feasible points but preserves at least one globally optimal solution.

An important special case of this idea arises when applying it to the box constraints $L_i \leq x_i \leq U_i$: if $L_i \leq x_i$ is active at the optimum of (22) with dual multiplier $\lambda_i^L > 0$, then we can update the upper bound U_i via

$$U_i := \min \left\{ U_i, L_i + \frac{UB - LB}{\lambda_i^L} \right\}.$$

Analogously, if $x_i \leq U_i$ is active with dual multiplier $\lambda_i^U > 0$, then we can update the lower bound L_i via

$$L_i := \max \left\{ L_i, U_i - \frac{UB - LB}{\lambda_i^U} \right\}.$$

Additionally, we can exploit the non-convex constraint $X = xx^\top$ in Problem (17) by applying the same idea to the main diagonal of X .

Lemma 1. *Let $i \in \{1, \dots, n\}$. If the constraint $X_{ii} \geq 1$ is active at the optimal solution of (22) with dual multiplier $\lambda > 0$, then we can update L_i and U_i via*

$$L_i := \max \left\{ L_i, -\sqrt{1 + \frac{UB - LB}{\lambda}} \right\}, \quad U_i := \min \left\{ U_i, \sqrt{1 + \frac{UB - LB}{\lambda}} \right\}.$$

Proof. We rewrite the constraint $X_{ii} \geq 1$ as $-X_{ii} + 1 \leq 0$. Using (23), the constraint

$$-X_{ii} + 1 \geq -\frac{UB - LB}{\lambda} \quad \Leftrightarrow \quad X_{ii} \leq 1 + \frac{UB - LB}{\lambda} =: \delta$$

preserves at least one globally optimal solution and can be added to the SDP relaxation (22) and the non-convex Problem (19). Moreover, $x_i^2 = X_{ii}$ must hold in any feasible solution of Problem (19). Thus, the constraints $-\sqrt{\delta} \leq x_i \leq \sqrt{\delta}$ also preserve at least one globally optimal solution. \square

Furthermore, our SDP relaxation (22) includes constraints of the form $X_{ii} \leq \max\{L_i^2, U_i^2\}$, which facilitate further tightening of the box constraints.

Lemma 2. *Let $i \in \{1, \dots, n\}$. Assume that a constraint of type $X_{ii} \leq \gamma$ is active at the optimal solution of (22) with dual multiplier $\lambda > 0$ such that $p := \gamma - \frac{UB - LB}{\lambda} \geq 1$. Then the following holds:*

- (i) If $L_i > -\sqrt{p}$, then we can update L_i via $L_i := \max\{L_i, \sqrt{p}\}$.
- (ii) If $U_i < \sqrt{p}$, then we can update U_i via $U_i := \min\{U_i, -\sqrt{p}\}$.

Proof. Applying (23) to the constraint $X_{ii} - \gamma \leq 0$ yields the new constraint

$$X_{ii} - \gamma \geq -\frac{UB - LB}{\lambda} \Leftrightarrow X_{ii} \geq p \geq 1.$$

We know that $x_i^2 = X_{ii}$ must hold in any feasible solution of Problem (19). If $x_i^2 \geq p$ and $-\sqrt{p} < L_i \leq x$, then certainly $x_i \geq \sqrt{p}$ must hold. Analogously, if $x_i^2 \geq p$ and $x_i \leq U_i < \sqrt{p}$, then $x_i \leq -\sqrt{p}$ must hold. \square

Lemma 2 establishes another scenario in which the degree of non-convexity can be reduced by fixing the sign of a variable. The main advantage of marginals-based bound tightening is that it is computationally inexpensive to apply. Thus, we apply it in every cutting-plane iteration after solving the SDP relaxation (22) and before separating violated RLT inequalities (21).

Overall, our bounding procedure involves four steps:

1. Box constraints computation by solving problems (18) whenever the global upper bound has been updated.
2. Solution of the basic SDP relaxation (20).
3. Cutting-plane algorithm for adding violated RLT inequalities (21) and solution of the corresponding SDP problem (22).
4. Improvement of box constraints using marginals-based bound tightening.

During the cutting-plane approach, we ensure that the sizes of SDPs remain manageable by removing (almost) inactive RLT cuts at each iteration. Moreover, we impose a minimum violation of any cut to be added to the relaxation and restrict the number of new cuts per iteration. We use the SDP solution at each iteration to apply the primal heuristic described in Section 4.2. The cutting-plane approach is stopped if the relative change of the lower bound compared to the last iteration is smaller than a fixed threshold. If necessary, we then apply the branching strategy presented in Section 4.3. In Section 6.3, we report a numerical comparison of different lower bounding approaches that confirms the effectiveness of our approach.

4.2 Primal heuristic

An essential component of any branch-and-bound methodology is the incorporation of primal heuristics to find good primal feasible solutions. In our case, any feasible solution of (12) yields an upper bound. Since Problem (12) involves continuous variables only, finding high-quality upper bounds can be difficult and time-consuming. However, producing nearly optimal upper bounds early in the branch-and-bound approach is particularly crucial for the overall efficiency of our approach. Firstly, solving SDPs is a relatively expensive task to do. Exploring fewer branch-and-bound nodes is always beneficial and leads to a noticeable speedup. Secondly, stronger upper bounds also allow us to compute tighter box constraints on each variable by (re-)solving the convex QCQPs (18). This again improves the RLT inequalities (21) and eventually leads to stronger lower bounds, reducing the optimality gap. Thirdly, marginals-based bound

tightening also uses the best-known upper bound, yielding stronger box constraints if better upper bounds are known.

Let (\hat{x}, \hat{X}) be the optimal solution of (22). Unless (\hat{x}, \hat{X}) forms a rank-one solution, i.e., $\hat{X} = \hat{x}\hat{x}^\top$ holds, \hat{x} is not feasible for the non-convex problem (12). Even if we neglect the balancing constraint (11), we would most likely get a solution of poor quality by just projecting each entry \hat{x}_i of \hat{x} onto the feasible region.

However, it is possible to improve any solution $\bar{x} \in \mathbb{R}^n$ that is feasible for (12) by constructing a labeling vector $\bar{y} \in \{-1, +1\}^n$ with entries $\bar{y}_i = \text{sign}(\bar{x}_i)$ for $i = 1, \dots, n$, and then solving the convex QP

$$\begin{aligned} \min_x \quad & x^\top C x \\ \text{s. t.} \quad & \bar{y}_i x_i \geq 1, \quad i = 1, \dots, n, \\ & \frac{1}{(n-l)} \sum_{i=l+1}^n x_i = \frac{1}{l} \sum_{i=1}^l y_i, \\ & x \in \mathbb{R}^n. \end{aligned} \tag{24}$$

The optimal solution of (24) will be feasible for (12), and it is the best solution one can get with respect to the fixed labeling vector \bar{y} . Solving the QP (24) is a non-trivial task within a heuristic. Still, it allows us to exploit the combinatorial structure of the problem: we now only have to find suitable labeling vectors with entries in $\{-1, +1\}$, which is much easier than directly finding feasible solutions with continuous entries.

Like suggested in [14], we exploit the optimal SDP solution (\hat{x}, \hat{X}) of (22) and first construct a labeling vector \bar{y} with entries $\bar{y}_i = \text{sign}(\hat{x}_i)$ for $i = 1, \dots, n$. We then solve the convex QP (24) with this labeling vector and obtain an upper bound on the non-convex problem (12). However, it turns out that a solution found this way can often be improved. To do so, we use a two-opt local search approach, which we present below.

Suppose that $\bar{x} \in \mathbb{R}^n$ is feasible for (12). The idea is to improve \bar{x} by selecting two variables x_i and x_j with $i, j \in \{l+1, \dots, n\}$, $i < j$, and then to solve Problem (12) with respect to x_i and x_j only, while keeping all other variables fixed at their values in \bar{x} . If doing so, Problem (12) reduces to

$$\begin{aligned} \min_{x_i, x_j} \quad & \begin{pmatrix} x_i \\ x_j \end{pmatrix}^\top \begin{pmatrix} C_{ii} & C_{ij} \\ C_{ij} & C_{jj} \end{pmatrix} \begin{pmatrix} x_i \\ x_j \end{pmatrix} + 2 \begin{pmatrix} \eta_i \\ \eta_j \end{pmatrix}^\top \begin{pmatrix} x_i \\ x_j \end{pmatrix} \\ \text{s. t.} \quad & x_i^2 \geq 1, \\ & x_j^2 \geq 1, \\ & x_i + x_j = k, \\ & x_i, x_j \in \mathbb{R}, \end{aligned} \tag{25}$$

where $\eta_i = \sum_{k \neq i, j}^n C_{ki} \bar{x}_k$, $\eta_j = \sum_{k \neq i, j}^n C_{kj} \bar{x}_k$, and $k = \bar{x}_i + \bar{x}_j$. Problem (25) still is a non-convex optimization problem, but we can solve it efficiently, as shown in the next proposition.

Proposition 2. *Problem (25) admits a global minimum, and this minimum can be computed analytically.*

Proof. We can eliminate the variable x_i by substituting $x_i = k - x_j$. This gives us a univariate optimization problem of the form

$$\begin{aligned} \min_{x_j} \quad & ax_j^2 + bx_j + c \\ \text{s. t.} \quad & g_1(x_j) = x_j^2 \geq 1, \\ & g_2(x_j) = (k - x_j)^2 \geq 1, \\ & x_j \in \mathbb{R}, \end{aligned} \tag{26}$$

where $a = C_{ii} + C_{jj} - 2C_{ij} > 0$, $b = 2k(C_{ij} - C_{ii}) - 2\eta_i + 2\eta_j$, and $c = C_{ii} + 2kg_i$. The objective function is quadratic and positive definite. Therefore, it is coercive and admits a global minimum. Thus, the global minimum will be a point at which the minimum objective value among all candidates derived by necessary optimality conditions is attained. The Lagrangian of (26) is given by

$$\mathcal{L}(x_j; \lambda_1, \lambda_2) = ax_j^2 + bx_j + c - \lambda_1(x_j^2 - 1) - \lambda_2((k - x_j)^2 - 1), \tag{27}$$

where λ_1 and λ_2 are Lagrange multipliers corresponding to the inequality constraints. The KKT conditions are

$$2ax_j + b - 2\lambda_1 x_j + 2\lambda_2(k - x_j) = 0, \tag{28}$$

$$\lambda_1(x_j^2 - 1) = 0, \tag{29}$$

$$\lambda_2((k - x_j)^2 - 1) = 0, \tag{30}$$

$$x_j^2 \geq 1, \tag{31}$$

$$(k - x_j)^2 \geq 1, \tag{32}$$

$$\lambda_1, \lambda_2 \geq 0. \tag{33}$$

Given the two constraints, there are four cases:

1. If $\lambda_1 = \lambda_2 = 0$, then no constraint is active. Then we get $x_j = -\frac{b}{2a}$ due to (28). Since this is the unconstrained global minimum, this solution is optimal if it is feasible, i.e., it satisfies (31) and (32).
2. Suppose $\lambda_1 > 0$ and $\lambda_2 = 0$. We get $x_j \in \{-1, +1\}$ due to (29). Then the LICQ constraint qualification holds since $\frac{\partial g_1}{\partial x_j} = 2x_j \neq 0$. Moreover, solving (28) for λ_1 yields $\lambda_1 = a + \frac{b}{2x_j} = a + \frac{b}{2}x_j$. For both candidates $x_j = -1$ and $x_j = +1$, we can check whether they are KKT points, i.e., λ_1 is nonnegative and (32) holds.
3. Suppose $\lambda_1 = 0$ and $\lambda_2 > 0$. We get $x_j \in \{k - 1, k + 1\}$ due to (30). Again, the LICQ constraint qualification holds since $\frac{\partial g_2}{\partial x_j} = -2(k - x_j) \neq 0$. Solving (28) for λ_2 yields $\lambda_2 = \frac{2ax_j + b}{2(k - x_j)}$. For both candidates, $x_j = k - 1$ and $x_j = k + 1$, we can check whether they are KKT points, i.e., λ_2 is nonnegative and (31) holds.

4. Suppose $\lambda_1 > 0$ and $\lambda_2 > 0$. We get $x_j \in \{-1, +1\}$ from (29) and $x_j \in \{k-1, k+1\}$ from (30). This can only be true if $k \in \{-2, 0, +2\}$. In this case, the point satisfies the Fritz John optimality conditions. Hence, it is a candidate for optimality.

The global minimum of Problem (25) is the candidate that achieves the minimum objective value. \square

We apply the two-opt local search in the following way. We start with a feasible solution $\bar{x} \in \mathbb{R}^n$ of Problem (12), and then loop through all possible pairs $\{i, j\}$ of unlabeled data points. For any pair, if the optimal solution of Problem (25) is better than the solution (\bar{x}_i, \bar{x}_j) , we immediately update \bar{x} and proceed with this updated solution. If all pairs have been tested and no improvement was found, we are done. Otherwise, we first update \bar{x} by solving the convex QP (24) using the labeling vector \bar{y} with entries $\bar{y}_i = \text{sign}(\bar{x}_i)$ for $i = 1, \dots, n$, and then we check all pairs $\{i, j\}$ for any improvement again. The pseudocode of this two-opt local search heuristic is given in Algorithm 1.

Algorithm 1 Two-opt local search heuristic

Input: Feasible solution $\bar{x} \in \mathbb{R}^n$ of Problem (12).

1. For every pair $\{i, j\}$ of unlabeled data points:
 - 1.1. Compute an optimal solution x_i, x_j of Problem (25) with respect to \bar{x} and the pair $\{i, j\}$.
 - 1.2. If the solution x_i, x_j differs from \bar{x}_i, \bar{x}_j , then update \bar{x}_i to x_i and \bar{x}_j to x_j .
2. If \bar{x} was updated in the last execution of *Step 1*, then compute a new vector \bar{x} by solving Problem (24) with respect to the labeling vector \bar{y} with entries $\bar{y}_i = \text{sign}(\bar{x}_i)$ for $i = 1, \dots, n$, and go to *Step 1*.

Output: Labeling vector \bar{y} and upper bound $UB = \bar{x}^\top C \bar{x}$.

4.3 Branching strategy

Problem (12) is a continuous optimization problem, but it is possible to enumerate all the solutions. Note that the Problem (12) becomes convex when all unlabeled data points have been labeled. Therefore, we select an unlabeled data point and derive two children corresponding to the two possible labels. In practice, labeling a point is equivalent to setting either the lower bound to $L_i = 1$ ($y_i = 1$) or the upper bound to $U_i = -1$ ($y_i = -1$). At a given node, some unlabeled points have already been assigned a label. This yields a binary enumeration tree where nodes are associated with a fixed partial labeling of the unlabeled dataset, and the two children correspond to the labeling of some new unlabeled point.

The key question is how to select, at any branching step, a data point to label. We explore different options, and all of them exploit the solution of our SDP relaxation (22) at the current node. To select interesting candidates, we do some preliminary considerations. Given the solution (\bar{x}, \bar{X}) of the SDP relaxation at the end of the

cutting-plane algorithm, we consider the labeling $\bar{y}_i = \text{sign}(\bar{x}_i)$ for $i = l + 1, \dots, n$ and solve the convex QP (24). Let x^* be the optimal solution of this problem.

We focus on the indices of unlabeled data points that satisfy $x_i^* = 1$ since they correspond to data points near the boundary of the decision function and, therefore, are more relevant. Moreover, we consider data points where the label assigned by the SDP solution appears to be undecided, i.e., $\bar{x}_i \in (-1, 1)$, hoping to achieve a bound improvement in both child nodes. Indeed, we restrict the candidates for branching to the set

$$\mathcal{U} = \{i = l + 1, \dots, n : x_i^* = 1 \text{ and } |\bar{x}_i| < 1\}.$$

To select the branching variable, we evaluate different measures that could help identify the variable leading to the largest bound improvement. We consider the approximation error, a quality measure that can be computed in various ways. In particular, we know that at the optimum $X_{ij} = x_i x_j$ must hold for all $i, j = 1, \dots, n$. The goal then is to label the point i that maximizes the approximation error, assuming that a larger approximation error indicates room for improvement on that variable. We consider four measures of the approximation error for variable $i \in \mathcal{U}$:

$$\begin{aligned} a_i^1 &= \sum_{j=1}^n (\bar{x}_i \bar{x}_j - \bar{X}_{ij}), & a_i^2 &= \sum_{j=1}^n |\bar{x}_i \bar{x}_j - \bar{X}_{ij}|, \\ a_i^3 &= \sum_{j=1}^n C_{ij} (\bar{x}_i \bar{x}_j - \bar{X}_{ij}), & a_i^4 &= \sum_{j=1}^n |C_{ij} (\bar{x}_i \bar{x}_j - \bar{X}_{ij})|. \end{aligned}$$

Another interesting measure of “undecidedness” is the box size around the variable x_i . Given that the point is unlabeled, we know that $L_i \leq -1$ and $U_i \geq 1$ must hold. If we select the data point i for branching, then we have:

- In the child where we choose the label $y_i = 1$, we set $L_i = 1$, thereby reducing the box by the positive amount $1 - L_i$.
- In the child where we choose the label $y_i = -1$, we set $U_i = -1$, reducing the box by the positive amount $1 + U_i$.

The intuition here is that the bound improvement is correlated with the reduction of the feasible set in the two children. Consequently, another interesting measure (the larger, the better) is defined as:

$$b_i = \min_{i \in \mathcal{U}} \{1 - L_i, 1 + U_i\}.$$

We then rank all data points in \mathcal{U} in decreasing order with respect to $a_i^1, a_i^2, a_i^3, a_i^4$, and b_i , summing up all the positions in the ranking. The branching variable is selected as the one with the lowest cumulative score.

The pseudocode of the overall branch-and-cut algorithm is given in Algorithm 2 and uses all our ingredients. Steps 5.1–5.6 in Algorithm 2 are executed sequentially for each node of the B&B tree. Consequently, the complexity per node is dominated by solving the SDP relaxation, which has a complexity of $\mathcal{O}(n^{3.5})$ and is performed as many times as the number of cutting-plane iterations. Whenever the box constraints

are updated, up to $2n$ convex QCQPs are solved using interior-point methods, each with a complexity of $\mathcal{O}(n^3)$.

Algorithm 2 Branch-and-cut algorithm for S3VM

Input: Kernel matrix \bar{K} , penalty parameters $C_l > 0$ and $C_u > 0$, labels $\{y_i\}_{i=1}^l$, upper bound UB , optimality tolerance $\varepsilon \geq 0$.

1. Set $L_i = 1$, $U_i = \infty$ if $y_i = 1$, $L_i = -\infty$, $U_i = -1$ if $y_i = -1$ for $i = 1, \dots, l$. Set $L_i = -\infty$, $U_i = \infty$ for $i = l + 1, \dots, n$.
2. Compute valid box constraints L_i and U_i for $i = 1, \dots, n$.
3. Let P_0 be the initial S3VM problem and set $\mathcal{Q} = \{P_0\}$.
4. Let $(y^u)^*$ be a labeling with objective function value $v^* = UB$.
5. While \mathcal{Q} is not empty:
 - 5.1. Select and remove problem P from \mathcal{Q} .
 - 5.2. Compute a lower bound LB for problem P by solving its SDP relaxation.
 - 5.3. If $v^* < \infty$ and $(v^* - LB)/v^* \leq \varepsilon$, go to *Step 5*.
 - 5.4. From the solution of the SDP relaxation, get a labeling y^u and an upper bound UB by running the two-opt local search heuristic in Algorithm 1. If $UB < v^*$, then set $v^* \leftarrow UB$, $(y^u)^* \leftarrow y^u$, update L_i and U_i for $i = 1, \dots, n$, apply bound tightening, and go to *Step 5.2*.
 - 5.5. Search for violated RLT inequalities. If any are found, add them to the current SDP relaxation, and go to *Step 5.2*. If no violated RLT inequality is found, or the lower bound did not improve, go to *Step 5.6*.
 - 5.6. Select an unlabeled data point with index i and partition problem P into two subproblems: one with $y_i = -1$ and the other with $y_i = 1$. Add each subproblem to \mathcal{Q} and go to *Step 5*.

Output: Labeling vector $(y^u)^*$ with objective value v^* .

Remark 3. *Algorithm 2 converges in a finite number of steps, even for $\varepsilon = 0$, due to the finiteness of the branch-and-bound tree. Each branch-and-bound node corresponds to a partial labeling of the dataset, and its two children represent labelings of different unlabeled points. The root of the tree contains only the original set of labeled examples. Each leaf in the tree represents a complete labeling of the dataset. Consequently, the problem is convex at the leaf nodes. This implies that Algorithm 2 terminates after exploring at most 2^{n-l} nodes, independently of the quality of lower and upper bounds. The effect of our machinery is to significantly reduce the number of nodes required to achieve nearly optimal solutions (where $\epsilon > 0$), as demonstrated by the computational results in Section 6.*

5 Ideal Kernel

When solving S3VM problems, the main goal is identifying the underlying ground-truth labels. The S3VM objective function may yield a solution far from the ground truth if the clustering assumption is not met or if hyperparameters are inadequately selected, as discussed by Chapelle et al. [6]. Therefore, an interesting question arises: is

there a kernel function that ensures that the S3VM objective function aligns with the ground truth while simultaneously making the SDP relaxation tight? The natural candidate for such a function is the ideal kernel, which establishes a class-based similarity score capable of perfectly discriminating between both classes. However, its analytical expression remains unknown and is dependent on the dataset. Assume that the classification outcome is available, i.e., we know $\gamma = [y_1, \dots, y_l, y_{l+1}^{gt}, \dots, y_n^{gt}]^\top$, where y_i^{gt} is the ground-truth label for the unlabeled data points. An example of an ideal kernel function is $\bar{K} = \gamma\gamma^\top$, where $\bar{k}(x_i, x_j) = -1$ if $\gamma_i \neq \gamma_j$ and $\bar{k}(x_i, x_j) = 1$ if $\gamma_i = \gamma_j$. This ensures that within-class distances in the feature space are zero and between-class distances are positive. Indeed, by applying the kernel trick, one can easily verify that

$$\|\phi(x_i) - \phi(x_j)\|^2 = \bar{k}(x_i, x_i) - 2\bar{k}(x_i, x_j) + \bar{k}(x_j, x_j) = \begin{cases} 0 & \text{if } \gamma_i = \gamma_j, \\ 4 & \text{if } \gamma_i \neq \gamma_j. \end{cases}$$

If we set $\bar{K} = \gamma\gamma^\top$, we can prove that for any positive values of the penalty parameters C_l and C_u , the global minimum of Problem (8) recovers the ground-truth classification. Furthermore, the SDP relaxation (15) is tight.

Proposition 3. *Given $C_l, C_u > 0$, let $\bar{K} = \gamma\gamma^\top$, then the global minimum of Problem (8) is $v^* = \gamma$, and $(\gamma, \gamma\gamma^\top)$ is the optimal solution of Problem (15).*

Proof. Assume that $\bar{K} = \gamma\gamma^\top$. Then the cost matrix of Problem (8) can be explicitly computed by the Sherman-Morrison formula

$$C = (D + \gamma\gamma^\top)^{-1} = D^{-1} - \frac{D^{-1}\gamma\gamma^\top D^{-1}}{1 + \gamma^\top D^{-1}\gamma},$$

where

$$D = \begin{bmatrix} \frac{1}{2C_l}I_l & 0_{l \times (n-l)} \\ 0_{(n-l) \times l} & \frac{1}{2C_u}I_{n-l} \end{bmatrix}, \quad D^{-1} = \begin{bmatrix} 2C_l I_l & 0_{l \times (n-l)} \\ 0_{(n-l) \times l} & 2C_u I_{n-l} \end{bmatrix}.$$

Indeed, the objective function of Problem (8) can be expressed as

$$v^\top (D + \gamma\gamma^\top)^{-1} v = v^\top D^{-1} v - \frac{v^\top D^{-1} \gamma \gamma^\top D^{-1} v}{1 + \gamma^\top D^{-1} \gamma}.$$

By setting $z = \sqrt{D^{-1}}v$ and $\beta = \sqrt{D^{-1}}\gamma$, Problem (8) can be rewritten as:

$$\begin{aligned} \min_z \quad & \|z\|^2 - \frac{(z^\top \beta)^2}{1 + \beta^\top \beta} \\ \text{s. t.} \quad & y_i z_i \geq \sqrt{2C_l}, \quad i = 1, \dots, l, \\ & z_i^2 \geq 2C_u, \quad i = l+1, \dots, n, \\ & z \in \mathbb{R}^n. \end{aligned} \tag{34}$$

Let $\lambda \in \mathbb{R}^n$ be the vector of multipliers associated with the inequality constraints. Then, we can write the (necessary) KKT conditions for Problem (34) as

$$2z_i - 2\frac{z^\top \beta}{1 + \|\beta\|^2}\beta - \lambda_i y_i = 0, \quad i = 1, \dots, l, \quad (35)$$

$$2z_i - 2\frac{z^\top \beta}{1 + \|\beta\|^2}\beta - 2\lambda_i z_i = 0, \quad i = l + 1, \dots, n, \quad (36)$$

$$\lambda_i (y_i z_i - \sqrt{2C_l}) = 0, \quad i = 1, \dots, l, \quad (37)$$

$$\lambda_i (z_i^2 - 2C_u) = 0, \quad i = l + 1, \dots, n, \quad (38)$$

$$\lambda_i \geq 0, \quad i = 1, \dots, n. \quad (39)$$

Now, consider the point \hat{z} such that all the constraints in (34) are active, that is

$$\begin{aligned} \hat{z}_i &= y_i \sqrt{2C_l}, \quad i = 1, \dots, l \\ \hat{z}_i^2 &= 2C_u, \quad i = l + 1, \dots, n. \end{aligned}$$

The second equation implies that either $\hat{z}_i = \sqrt{2C_u}$ or $\hat{z}_i = -\sqrt{2C_u}$ for $i = l + 1, \dots, n$, and we have that $\|\hat{z}\|^2 = \|\beta\|^2$. By (34), the objective function value becomes

$$\|\hat{z}\|^2 - \frac{(\beta^\top \hat{z})^2}{1 + \|\beta\|^2} = \|\beta\|^2 - \frac{(\sum_{i=1}^n \hat{z}_i \beta_i)^2}{1 + \|\beta\|^2},$$

which is minimized when the term $\sum_{i=1}^n \hat{z}_i \beta_i$ is maximized. The term is maximal when \hat{z}_i and β_i have the same sign, meaning that $\hat{z}_i = y_i^{gt} \sqrt{2C_u} = \beta_i$. Then, the objective function value in \hat{z} is

$$\|\hat{z}\|^2 - \frac{(\beta^\top \hat{z})^2}{1 + \|\beta\|^2} = \frac{1}{1 + \beta^\top \beta}.$$

By setting $\hat{z} = \beta$ in (35)–(36), we get

$$\begin{aligned} y_i \lambda_i &= 2\beta_i - 2\frac{\|\beta\|^2}{1 + \|\beta\|^2}\beta_i, \quad i = 1, \dots, l, \\ 2\beta_i^2 - 2\frac{\|\beta\|^2}{1 + \beta^\top \beta}\beta_i^2 - 2\lambda_i \beta_i^2 &= 0, \quad i = l + 1, \dots, n, \end{aligned}$$

where the second equation is obtained by multiplying (36) by \hat{z}_i . Then, we have

$$\begin{aligned} \hat{\lambda}_i &= \frac{2\sqrt{2C_l}}{1 + \|\beta\|^2} > 0, \quad i = 1, \dots, l, \\ \hat{\lambda}_i &= \frac{2\sqrt{2C_u}}{1 + \|\beta\|^2} > 0, \quad i = l + 1, \dots, n, \end{aligned}$$

which implies that the pair $(\hat{z}, \hat{\lambda})$ is a KKT point. Looking at the objective function of Problem (34) and using the Cauchy-Schwartz inequality $(z^\top \beta)^2 \leq \|z\|^2 \|\beta\|^2$, we get

$$f(z) = \|z\|^2 - \frac{(\beta^\top z)^2}{1 + \beta^\top \beta} \geq \frac{\|z\|^2}{1 + \|\beta\|^2}.$$

At \hat{z} , we get $f(\hat{z}) = \frac{\|\hat{z}\|^2}{1 + \|\hat{\beta}\|^2}$, so the minimum is achieved, and the point is a global minimum of Problem (34).

Finally, it remains to show that the SDP relaxation (20) is tight. Plugging the ideal kernel into the objective function of (20), we get

$$\begin{aligned} \min_{\bar{X}} \quad & \left\langle D^{-1} - \frac{D^{-1} \gamma \gamma^\top D^{-1}}{1 + \gamma^\top D^{-1} \gamma}, X \right\rangle \\ \text{s. t.} \quad & L_i \leq x_i \leq U_i, \quad i = 1, \dots, n, \\ & 1 \leq X_{ii} \leq \max\{L_i^2, U_i^2\}, \quad i = 1, \dots, n, \\ & \bar{X} = \begin{pmatrix} X & x \\ x^\top & 1 \end{pmatrix} \succeq 0, \quad x \in \mathbb{R}^n, \quad X \in \mathbb{S}^n. \end{aligned} \tag{40}$$

We know that the point $(\gamma, \gamma \gamma^\top)$ is feasible for Problem (40), and that the objective function satisfies

$$\left\langle D^{-1} - \frac{D^{-1} \gamma \gamma^\top D^{-1}}{1 + \gamma^\top D^{-1} \gamma}, \gamma \gamma^\top \right\rangle = \gamma^\top D^{-1} \gamma - \frac{(\gamma^\top D^{-1} \gamma)^2}{1 + \gamma^\top D^{-1} \gamma} = \frac{\|\hat{z}\|^2}{1 + \|\hat{\beta}\|^2},$$

where the last equality derives from $\hat{z} = \beta = \sqrt{D^{-1} \gamma}$. Therefore, the relaxation is optimal. \square

Although Proposition 3 provides theoretical insights into the recovery properties of the SDP relaxation (20), the ideal kernel is not available in practice. However, the concept of an ideal kernel is useful because it defines how a kernel should be in order to achieve perfect classification. Indeed, we can expect a strong correlation between the objective function of the S3VM problem and the ground-truth labels, given that the kernel function is “close” to a kernel that effectively discriminates between the two classes. In this setting, the SDP relaxation (20) is expected to provide a strong bound that is further improved when RLT inequalities (21) are added.

The theoretical result linking bound quality to kernel effectiveness is supported by the numerical results in Section 6.4. Indeed, the only instances where we have huge gaps correspond to a wrong choice of the kernel function.

6 Numerical Results

This section provides the implementation details, outlines the details of the experimental setup, and thoroughly analyzes the computational results.

6.1 Implementation details

Our SDP-based B&B algorithm is implemented in **Julia** (version 1.9.4), and **JuMP** [26] is used to formulate all occurring optimization problems. We use **MOSEK** (version 10.1.8) to solve SDPs within our bounding routine and **Gurobi** (version 10.0) to solve QCQPs for estimating box constraints. All experiments are performed on a machine with an Intel(R) Core(TM) i7-12700H processor with 14 cores clocked at 3.50 GHz, 16 GB of RAM, and Ubuntu 22.04 as the operating system. As for the cutting-plane approach, we add up to $5n$ of the most violated RLT inequalities at each iteration. In our numerical tests, we set the tolerance for checking the violation to 10^{-2} . Furthermore, the tolerance for removing inactive cuts is set to 10^{-4} . We stop the cutting-plane procedure when the relative difference between consecutive lower bounds is less than 10^{-3} and explore the B&B tree using the best-first search strategy.

As an optimality measure, we use the percentage gap computed as $\varepsilon = ((UB - LB)/UB) \times 100$, where UB is the best known upper bound and LB is the lower bound. Although our branch-and-bound algorithm is exact and capable of producing optimality certificates for any given $\varepsilon > 0$ in finite time, we stop our algorithm when ε is less than 0.1%. This allows us to obtain nearly optimal solutions. Moreover, the remaining gap of 0.1% is negligible in machine learning applications.

To enhance reproducibility, the source code has been made publicly available through the link <https://github.com/jschwiddessen/SDP-S3VM>. This repository provides all the tools to verify, build upon, and improve our global S3VM solver.

6.2 Test instances

To assess the effectiveness of our proposed branch-and-cut algorithm, we test it on various binary classification datasets. More precisely, we consider three artificial datasets, **art_100**, **art_150**, and **2moons** and several real-world datasets taken from the literature¹. Table 1 provides details on these datasets, including the number of data points (n), the number of features (d), and the total number of positive and negative examples, $(\# + 1)$ and $(\# - 1)$ respectively. We standardize the features such that each feature has zero mean and unit standard deviation. From each dataset, we derive different instances for our problem. Specifically, we randomly select a percentage $p \in \{10\%, 20\%, 30\%\}$ of data points to build the set of labeled examples while preserving the percentage of samples for each class. All the remaining points are treated as unlabeled. We consider three different random seeds for selecting the labeled data points to diversify the set of labeled examples. Indeed, the quality of the labeled data points plays a crucial role in guiding the optimization process and shaping the decision boundary between different classes.

6.3 Lower bound comparison

In this section, we conduct a comparative analysis between our lower bound presented in Section 4.1 and the ones derived from the convex relaxations described in Section 3.2. Specifically, the following relaxations are considered:

¹<https://archive.ics.uci.edu/>

Table 1: Characteristics of the tested datasets.

Dataset	n	d	$\# + 1$	$\# - 1$
art_100	100	2	50	50
art_150	150	2	77	73
connectionist	208	60	111	97
heart	270	13	120	150
2moons	300	2	150	150
ionosphere	351	33	126	225
PowerCons	360	144	180	180
GunPoint	451	150	223	228
arrhythmia	452	191	207	245
musk	476	166	207	269
wdbc	569	30	357	212

1. *QP*: The standard QP relaxation obtained by solving Problem (8) without the non-convex constraints $v_i^2 \geq 1$ for $i = 1, \dots, n$.
2. *QP-L*: The QP relaxation (13) where violations of the non-convex constraints are penalized in the objective function by means of Lagrangian multipliers. The multipliers are estimated by solving the auxiliary SDP (14).
3. *SDP*: The SDP relaxation (15).
4. *SDP-RLT*: The SDP relaxation (22) without the balancing constraint (11), where we apply bound tightening and add violated RLT cuts using our cutting-plane strategy. Box constraints $L_i \leq x_i \leq U_i$ are estimated by solving convex QCQPs of type (18) for all $i = 1, \dots, n$. The computation of a valid upper bound UB required for Problem (18) involves optimizing a supervised SVM only on the labeled data points and classifying the unlabeled data points. Thus, using this SVM labeling, UB is determined as the solution of (24) without the balancing constraint (9).

Note that, for this set of experiments, we neglect the balancing constraint (11) to stick with the original convex relaxations described in the literature. Since incorporating the balancing constraint involves adding only a single linear constraint, we expect no differences in terms of bound comparison or computational time. Computational results for the DNN presented in (16) are omitted due to long computing times and memory requirements, even for small-scale instances. Additionally, based on computational findings in [14], the DNN relaxation yields a marginally improved bound compared to the standard SDP but at significantly higher computational costs. Given that branch-and-bound algorithms depend on both strong and computationally efficient bounds, further computations using the DNN relaxation (16) are not pursued, as it is impractical to integrate it into any branch-and-bound algorithm.

We select the radial basis function (RBF) kernel for all instances, defined as $K_{ij} = \exp(-\gamma \|x_i - x_j\|^2)$, where $x_i, x_j \in \mathbb{R}^d$ represent feature vectors in the input space. Here, we set $\gamma = 1/d$, $C_l = 1$, and $C_u = 0.2 \cdot (l/(n-l)) \cdot C_l$. We average the results across the three seeds for each dataset and each percentage of labeled data points. Table 2 presents, for each relaxation, the number of labeled data points l , the number of unlabeled data points $n-l$, the percentage gap with respect to the upper bound UB , and the computational time in seconds. Additionally, for the SDP-RLT relaxation, Table 2 includes the “Time Box” column, indicating the average time spent in seconds

for computing box constraints, and the “Iter” column, representing the average number of performed cutting-plane iterations. Table 2 shows the superiority of the lower bound produced by SDP-RLT. While the bounds obtained from QP, QP-L, and SDP are faster to compute, they exhibit notably larger gaps. The substantial improvement in the lower bound achieved through RLT cuts justifies the time invested in computing box constraints. Across all instances, the average gap is less than 0.5%, with only one instance exceeding 0.66%. Notably, SDP-RLT attains a zero gap in 35 out of 81 instances and maintains gaps below 0.01% in 46 instances (57% of all instances). This indicates that we successfully solve more than half of the instances at the root node with this standard parameter configuration.

6.4 Branch-and-cut results

In this section, we report numerical experiments of the overall branch-and-cut approach. To the best of our knowledge, the only exact algorithms for L2-norm S3VMs are the branch-and-bound methods introduced in [17] and [21]. Moreover, recent versions of Gurobi incorporate solvers for non-convex QCQPs and can solve problems of type (12). We specifically focus on comparing against Gurobi, as the branch-and-bound method in [21] uses the relaxation in (13) for the bounding routine, which has been demonstrated in Section 6.3 to be considerably weaker than our SDP-RLT relaxation. Moreover, the branch-and-bound approach proposed in [17] is only suitable for small instances ($n \leq 50$) since it relies on analytic bounds that are notably weak and require the exploration of a large portion of the branch-and-bound tree.

Following the related literature, we perform a k -fold cross-validation to determine the hyperparameters on only the set of labeled data points. By cross-validation, we choose the kernel function and the penalty parameter C_l for labeled data points. We set $k = 10$ for all datasets, except for **art100** and **art150**, where we set $k = 2$ due to the limited number of labeled data points. The penalty parameter for unlabeled data points C_u is set to $0.2 \cdot (l/(n-l)) \cdot C_l$. The factor $l/(n-l)$ balances the contribution of labeled and unlabeled data points, and we further diminish the influence of unlabeled data points by the factor 0.2 to give more weight to labeled data points.

The first set of experiments aims to understand how Gurobi behaves on different instances. We restrict to the smaller ones, that is, $n \leq 300$, and we set a time limit of 3600 seconds. In Table 3, we report the instance name, the number of labeled (l), and unlabeled data points ($n - l$). Then, for both Gurobi and our solver (SDP-S3VM), we report the average percentage gap (Gap [%]), the average computational time in seconds (Time [s]), and the number of instances solved to global optimality (Solved), ranging between 0 and 3. The computational results show that Gurobi encounters difficulties in closing the gap on most instances. Specifically, only 11 out of 45 instances are solved to optimality. As the number of unlabeled data points increases, the instances become more challenging, and the optimality gap becomes significantly larger after one hour of computation. On the other hand, our solver consistently outperforms Gurobi while solving 43 out of 45 instances and producing an average gap smaller than 1% on the two remaining instances of **connectionist**.

In Tables 4 and 5, we report the detailed performance of our solver on the small and large instances, respectively. Specifically, we show the performance of our B&B

Table 2: For each relaxation, we present the average percentage gap (Gap [%]) and the average computational time in seconds (Time [s]). This analysis is conducted for varying percentages of labeled data points, where l is set to be 10%, 20%, and 30% of the total number of data points, n . Additionally, for the SDP-RLT relaxation, we report the average time required for computing box constraints (Time Box [s]) and the average number of cutting-plane iterations (Iter).

Instance	l	$n - l$	QP		QP-L		SDP		SDP-RLT			
			Gap [%]	Time [s]	Gap [%]	Time [s]	Gap [%]	Time [s]	Time Box [s]	Gap [%]	Time [s]	Iter
2moons	30	270	10.70	0.09	10.60	0.58	3.59	0.57	11.86	0.00	7.57	3.00
2moons	60	240	7.97	0.09	9.12	0.64	3.41	0.56	12.45	0.00	7.35	3.00
2moons	90	210	7.86	0.09	11.12	0.59	4.04	0.54	11.12	0.00	7.31	3.00
arrhythmia	44	408	19.83	0.13	10.27	1.95	9.81	1.74	45.98	0.42	115.82	6.00
arrhythmia	90	362	18.41	0.14	11.66	1.76	11.38	1.71	43.54	0.41	97.73	5.67
arrhythmia	135	317	16.57	0.14	11.08	1.79	10.69	1.77	41.20	0.22	61.59	5.00
art100	10	90	13.80	0.00	10.82	0.06	1.89	0.06	0.48	0.03	0.70	3.00
art100	20	80	14.17	0.00	16.31	0.06	1.12	0.06	0.51	0.00	0.58	3.00
art100	30	70	10.01	0.01	10.99	0.06	3.18	0.07	0.48	0.01	0.67	3.00
art150	14	136	14.01	0.05	11.80	0.18	3.15	0.13	1.30	0.04	1.44	3.00
art150	29	121	11.52	0.07	12.67	0.22	4.44	0.15	1.59	0.00	1.69	3.00
art150	44	106	10.19	0.05	16.36	0.18	5.31	0.15	1.32	0.01	1.38	3.00
connectionist	20	188	21.40	0.08	7.93	0.29	6.39	0.27	3.21	0.19	6.13	4.00
connectionist	41	167	19.27	0.08	10.17	0.33	8.40	0.27	3.09	0.16	9.84	4.67
connectionist	62	146	18.29	0.07	11.54	0.35	9.98	0.27	3.05	0.45	9.03	4.67
GunPoint	44	407	10.99	0.15	8.81	1.60	7.90	1.54	47.15	0.00	57.56	4.00
GunPoint	89	362	10.39	0.16	9.55	1.78	8.58	1.55	46.59	0.04	55.44	4.00
GunPoint	134	317	10.36	0.14	9.99	1.82	9.02	1.56	43.90	0.01	50.60	4.00
heart	27	243	19.68	0.07	8.06	0.45	5.84	0.39	6.92	0.22	10.36	4.00
heart	54	216	15.90	0.09	9.48	0.49	6.96	0.38	6.96	0.08	13.93	4.33
heart	81	189	14.57	0.08	9.79	0.50	7.65	0.38	6.37	0.15	12.05	4.33
ionosphere	34	317	19.90	0.12	7.31	1.06	3.85	0.91	19.84	0.66	19.53	3.67
ionosphere	70	281	16.67	0.17	6.22	0.98	3.87	0.93	19.67	0.01	20.73	3.33
ionosphere	104	247	16.30	0.13	7.27	0.98	4.97	0.90	17.98	0.00	27.77	4.00
PowerCons	36	324	18.83	0.13	13.31	1.10	5.52	0.95	21.80	0.04	22.79	3.67
PowerCons	72	288	17.04	0.11	14.66	1.00	6.50	0.88	19.12	0.01	26.26	4.00
PowerCons	108	252	15.07	0.12	14.11	1.00	6.52	0.90	18.87	0.01	28.53	4.00

Table 3: Average gap and computational time for instances with $n \leq 300$ solved by Gurobi and our solver SDP-S3VM. For each instance, the gap and time are averaged over three different seeds with an increasing number of labeled data points ($p = 10\%, 20\%, 30\%$). We also report in column “Solved” the number of instances solved for a given dataset and the value of p .

Instance	l	$n - l$	Gurobi			SDP-S3VM		
			Gap [%]	Time [s]	Solved	Gap [%]	Time [s]	Solved
art100	10	90	7.37	3600	0	0.10	26.11	3
art100	20	80	3.09	2467.43	1	0.10	13.28	3
art100	30	70	3.27	2401.26	1	0.10	37.48	3
art150	14	136	8.44	3600	0	0.10	61.05	3
art150	29	121	2.72	1450.20	2	0.10	1.89	3
art150	44	106	2.52	2629.13	1	0.10	2.44	3
connectionist	20	188	16.83	3600	0	0.88	2587.20	1
connectionist	62	146	12.87	3600	0	0.10	248.07	3
connectionist	41	167	10.71	3600	0	0.10	104.95	3
heart	27	243	14.00	3600	0	0.10	38.89	3
heart	54	216	10.21	3600	0	0.10	64.45	3
heart	81	189	10.58	3600	0	0.10	16.22	3
2moons	30	270	6.52	3600	0	0.10	16.22	3
2moons	60	140	0.03	1023.52	3	0.10	22.07	3
2moons	90	210	0.05	1.95	3	0.10	21.50	3

approach, including the number of nodes (Nodes), the final gap (Gap [%]), and computational time (Time [s]). We also evaluate the quality of the produced solution in terms of accuracy. By accuracy, we mean the percentage of correctly labeled data points among the unlabeled ones. Indeed, we report the number of labeled (l) and unlabeled data points ($n - l$), the kernel, the penalty parameter for the labeled data points C_l ($C_u = 0.2 \cdot (l/(n - l)) \cdot C_l$), the percentage gap (Gap [%]), the number of nodes (Nodes), and the computational time in seconds. Furthermore, we report the accuracy on all unlabeled data points produced by our solution and the accuracy of the baseline, which is the accuracy on unlabeled data points obtained by a supervised SVM built using only labeled data points as a training set. We do not report the time required by the supervised SVM, as only one convex QP needs to be solved in this case, and the solution time is negligible even compared to the execution of an S3VM lower bound procedure. We set a time limit of 3600 seconds (one hour) on the small instances ($n \leq 300$) and a time limit of 10800 seconds (three hours) on the larger ones.

The computational results show that we solve 88 instances out of 99 to the required precision (gap less than 0.1%). On the remaining 11 instances, we hit the time limit. Overall, our method performs very well, with a low number of average nodes and closing many instances at the root node (39 out of 99 instances), confirming the high quality of our SDP bound. For the two instances of **connectionist** that we do not solve, we achieve a gap of 1.25% and 1.29% after one hour of computation. Among the large-scale instances, we do not solve nine instances, but we consistently achieve a gap of less than 2% except in four cases. These four instances include two from the **arrhythmia** dataset and two from the **musk** dataset. However, we can see that in all four instances, the cross-validation leads to a wrong choice of the kernel. Indeed, the best choice of the kernel was the RBF (chosen on all the other instances derived by the two datasets **arrhythmia** and **musk**), whereas on all four instances, the linear kernel

was chosen. This can be explained by the small number of labeled data points used for the cross-validation, which may lead to wrong choices. We will see in the following subsection that when choosing the RBF kernel, the gap decreases to values less than 1%, and the accuracy increases.

These examples show that solving an S3VM instance to optimality is influenced by various factors, such as the number of unlabeled data points, the chosen hyperparameters, and the kernel selection due to the potential violation of the clustering assumption for certain kernel choices [4]. Regardless of the challenges posed by solving a particular instance from a mathematical optimization perspective, the accuracy of the final labeling produced by the global minimum is influenced by the aforementioned choices. Further discussion on this aspect will be provided in the next section.

Table 4: In this table, we show the performance of our solver on small instances. We report the instance name, the number of labeled data points l , the number of unlabeled data points $n - l$, the kernel, the penalty parameter C_l , the percentage gap (Gap [%]), the number of nodes (Nodes), the computational time in seconds (Time [s]), the accuracy of the produced solution on the unlabeled data points (Acc. [%]), the accuracy of a supervised SVM built on the labeled data points and tested on the unlabeled ones (Base [%]). We highlight in boldface the labeling that achieves the highest accuracy on the unlabeled data points.

Instance	l	$n - l$	Kernel	C_l	Gap [%]	Nodes	Time [s]	Acc. [%]	Base [%]
art100	10	90	linear	0.1	0.1	3	11.39	94.44	94.44
art100	10	90	linear	0.1	0.1	11	13.47	95.56	96.67
art100	10	90	RBF	0.1	0.1	185	53.48	91.11	87.78
art100	20	80	linear	0.1	0.1	1	10.65	96.25	93.75
art100	20	80	linear	0.1	0.1	1	10.68	97.50	93.75
art100	20	80	RBF	0.1	0.1	27	18.52	90.00	87.50
art100	30	70	linear	0.1	0.1	1	10.77	95.71	92.86
art100	30	70	RBF	0.1	0.1	3	11.00	94.29	90.00
art100	30	70	RBF	0.1	0.1	53	26.54	94.29	87.14
art150	14	136	RBF	1.58	0.1	115	101.13	84.56	87.50
art150	14	136	linear	0.1	0.1	1	2.40	91.91	90.44
art150	14	136	RBF	0.1	0.1	11	8.92	86.76	83.82
art150	29	121	RBF	3.16	0.1	1	2.88	89.26	88.43
art150	29	121	RBF	0.1	0.1	219	168.61	90.91	87.60
art150	29	121	RBF	3.98	0.1	9	11.67	85.12	86.78
art150	44	106	linear	0.1	0.1	1	1.72	88.68	88.68
art150	44	106	linear	0.1	0.1	1	1.56	89.62	89.62
art150	44	106	linear	0.2	0.1	1	2.40	85.85	83.02
connectionist	20	188	linear	0.10	1.25	1448	3600	59.04	60.11
connectionist	20	188	linear	0.10	0.1	319	559.59	65.43	66.49
connectionist	20	188	RBF	1.26	1.29	1140	3600	69.15	69.68
connectionist	41	167	RBF	0.50	0.1	3	16.13	71.86	75.45
connectionist	41	167	RBF	0.10	0.1	263	518.69	59.88	62.87
connectionist	41	167	linear	0.10	0.1	129	209.38	74.25	73.65
connectionist	62	146	RBF	1.26	0.1	41	108.72	86.3	86.99
connectionist	62	146	RBF	0.63	0.1	77	188.95	71.23	71.92
connectionist	62	146	RBF	0.50	0.1	3	17.19	86.30	80.82
heart	27	243	RBF	0.10	0.1	3	23.12	81.89	80.25
heart	27	243	RBF	0.79	0.1	1	20.08	80.25	79.42
heart	27	243	linear	0.16	0.1	21	73.47	69.96	70.37
heart	54	216	RBF	0.10	0.1	1	11.49	83.33	82.41
heart	54	216	RBF	0.40	0.1	1	20.79	84.72	82.87
heart	54	216	linear	0.10	0.1	47	161.07	76.85	75.93
heart	81	189	RBF	0.10	0.1	1	11.75	85.19	85.19

heart	81	189	RBF	0.10	0.1	1	18.80	85.19	85.19
heart	81	189	RBF	0.10	0.1	1	18.12	84.13	83.07
2moons	30	270	RBF	2.51	0.1	1	33.71	97.78	97.04
2moons	30	270	RBF	0.10	0.1	1	29.25	87.04	87.04
2moons	30	270	RBF	0.50	0.1	1	30.10	91.85	92.22
2moons	60	240	RBF	3.98	0.1	1	21.77	100.00	100.00
2moons	60	240	RBF	3.98	0.1	1	21.62	100.00	100.00
2moons	60	240	RBF	1.26	0.1	1	22.83	97.92	97.92
2moons	90	210	RBF	3.16	0.1	1	21.38	100.00	100.00
2moons	90	210	RBF	2.51	0.1	1	21.15	100.00	100.00
2moons	90	210	RBF	1.26	0.1	1	21.97	97.62	97.62

Table 5: In this table, we show the performance of our solver on large instances. We report the instance name, the number of labeled data points l , the number of unlabeled data points $n - l$, the kernel, the penalty parameter C_l , the percentage gap (Gap [%]), the number of nodes (Nodes), the computational time in seconds (Time [s]), the accuracy of the produced solution on the unlabeled data points (Acc. [%]), the accuracy of a supervised SVM built on the labeled data points and tested on the unlabeled ones (Base [%]). We highlight in boldface the labeling that achieves the highest accuracy on the unlabeled data points.

Instance	l	$n - l$	Kernel	C_l	Gap [%]	Nodes	Time [s]	Acc. [%]	Base [%]
ionosphere	34	317	RBF	0.79	0.1	59	529.48	91.80	81.70
ionosphere	34	317	linear	0.40	0.1	73	492.74	88.33	88.96
ionosphere	34	317	linear	0.13	0.1	3	50.05	87.38	84.23
ionosphere	70	281	RBF	2.51	0.1	3	107.89	90.75	90.04
ionosphere	70	281	RBF	10.00	0.1	7	181.61	91.46	85.05
ionosphere	70	281	linear	0.16	0.1	1	43.55	88.61	87.54
ionosphere	104	247	RBF	2.51	0.1	5	128.45	90.28	90.69
ionosphere	104	247	linear	0.32	0.1	37	221.45	88.26	86.64
ionosphere	104	247	linear	0.16	0.1	1	56.87	89.47	90.69
PowerCons	36	324	RBF	1.26	0.1	11	139.97	95.06	93.83
PowerCons	36	324	RBF	1.58	0.1	1	45.20	95.37	96.30
PowerCons	36	324	linear	0.10	0.1	53	534.19	97.84	94.44
PowerCons	72	288	RBF	0.16	0.1	11	101.41	95.83	94.79
PowerCons	72	288	RBF	1.58	0.1	1	30.79	96.53	97.57
PowerCons	72	288	linear	0.10	0.1	55	375.76	98.61	97.57
PowerCons	108	252	linear	0.10	0.1	11	129.53	98.81	98.81
PowerCons	108	252	linear	0.10	0.1	15	109.83	98.81	99.21
PowerCons	108	252	linear	0.10	0.1	17	169.85	98.41	99.21
GunPoint	44	407	RBF	10.00	0.1	1	94.24	87.71	88.21
GunPoint	44	407	RBF	0.79	0.1	207	2925.41	84.03	87.96
GunPoint	44	407	RBF	0.79	0.1	7	318.37	88.94	86.98
GunPoint	89	362	RBF	3.98	0.1	1	130.63	95.58	96.13
GunPoint	89	362	RBF	7.94	0.1	1	138.84	95.03	94.75
GunPoint	89	362	RBF	3.16	0.1	1	98.54	93.09	92.54
GunPoint	134	317	RBF	3.16	0.1	1	88.93	95.58	96.53
GunPoint	134	317	RBF	5.01	0.1	1	60.82	94.01	94.32
GunPoint	134	317	RBF	10.00	0.1	23	484.11	91.80	92.43
arrhythmia	44	408	RBF	0.63	0.1	67	2463.22	72.30	65.93
arrhythmia	44	408	RBF	0.20	0.1	1	88.19	72.06	63.73
arrhythmia	44	408	linear	0.10	9.5	563	10800	69.12	69.61
arrhythmia	90	362	RBF	1.58	0.37	555	10800	74.31	70.72
arrhythmia	90	362	linear	0.32	10.91	532	10800	67.40	67.13
arrhythmia	90	362	RBF	1.26	0.18	371	10800	70.99	70.99
arrhythmia	135	317	RBF	2.00	0.56	632	10800	75.08	74.45
arrhythmia	135	317	RBF	0.25	0.1	79	2002.53	74.45	72.87
arrhythmia	135	317	RBF	3.98	1.88	415	10800	72.24	74.13

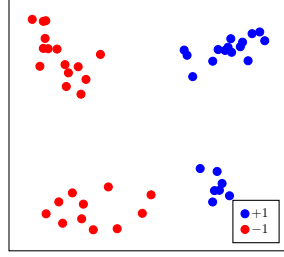
musk	46	430	linear	0.79	30.75	323	10800	70.23	69.30
musk	46	430	RBF	0.25	0.1	1	235.84	68.37	72.33
musk	46	430	linear	0.10	9.11	503	10800	67.44	66.51
musk	94	382	RBF	1.00	0.16	455	10800	80.63	81.68
musk	94	382	RBF	0.50	0.1	3	161.91	81.94	81.68
musk	94	382	RBF	0.25	0.14	421	10800	78.53	77.75
musk	142	334	RBF	2.00	0.1	265	4173.31	88.02	85.03
musk	142	334	RBF	6.31	1.16	583	10800	88.62	87.13
musk	142	334	RBF	0.79	0.1	645	7914.07	84.43	83.83
wdbc	56	513	linear	0.25	0.1	69	1398.81	96.30	95.32
wdbc	56	513	linear	0.10	0.1	3	210.55	94.74	94.93
wdbc	56	513	linear	0.10	0.1	1	193.61	96.88	96.88
wdbc	113	456	RBF	1.26	0.1	1	281.77	96.49	96.05
wdbc	113	456	linear	0.10	0.1	15	438.33	94.96	95.83
wdbc	113	456	RBF	5.01	0.1	11	381.48	96.05	96.05
wdbc	170	399	RBF	3.98	0.1	11	543.02	96.74	97.49
wdbc	170	399	RBF	0.32	0.1	1	279.65	94.49	94.99
wdbc	170	399	RBF	3.16	0.1	3	163.32	96.99	96.49

6.5 Machine learning perspective

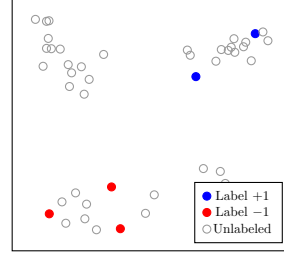
In this section, we discuss the obtained results from the machine learning point of view. Our method solves S3VM classification problems to global optimality, thus avoiding the issues related to the presence of local minima. However, this may not be enough to obtain good classification performance. Semi-supervised learning primarily aims to exploit unlabeled data to construct better classification algorithms. As it turns out, this is not always easy or even possible. As mentioned earlier, unlabeled data is only useful if it carries information for label prediction that is not contained in the labeled data alone or cannot be easily extracted from it. Moreover, we also remark that the clustering assumption is a crucial and necessary condition for semi-supervised learning to succeed. In other words, if the data points (both unlabeled and labeled) cannot be meaningfully clustered, it is impossible for a semi-supervised learning method to improve on a supervised learning one.

However, assuming that the problem is solved to global optimality, some issues can be fixed by either considering the balancing constraint or changing the hyperparameters. To begin, we illustrate the advantage of including the balancing constraint with an example, especially when the labeled data points lack sufficient information. Indeed, depending on the quality of labeled data points, fluctuation in accuracy can be experienced when minimizing the objective function of Problem (8), and the global minimum may perform poorly in terms of accuracy with respect to local minima with higher objective value. This can result from the inclination to cluster as many closely located points together as possible. Therefore, if the labeled data points are not informative enough, this may lead to collocating many unlabeled points in the same class, leading to poor accuracy.

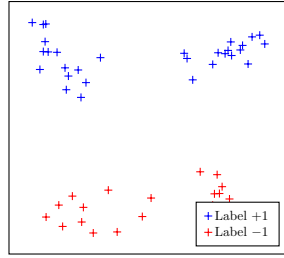
As an example, consider Figures 1a–1d. We have a small dataset of 50 data points in the plane, and the ground truth is reported in Figure 1a. Assume we have 10% of labeled data points that are the ones shown in Figure 1b. Then, if we solve Problem (8) to global optimality, we get the labeling of Figure 1c, which achieves an accuracy of 52% on the unlabeled data points. However, if we introduce the balancing constraint, the global minimum leads to the labeling in Figure 1d that perfectly recovers the ground truth (100% accuracy). The example in Figure 1a might be seen as an extreme



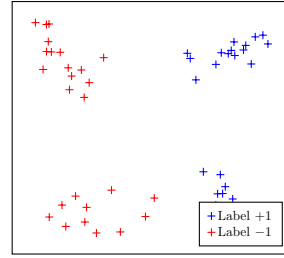
(a) Ground-truth classification



(b) Labeled and unlabeled data points



(c) Optimal S3VM solution



(d) Optimal S3VM solution with balancing

case, but our experience shows that omitting the balancing constraint (11) deteriorates the performance, even on real-world data. To demonstrate this behavior, we select two instances with less balanced class distribution, **ionosphere** and **heart**, and compare the results with and without the balancing constraint. Table 6 shows the accuracy on the unlabeled data points without the balancing constraint (column No Balancing [%]) and with it (column Balancing [%]). The hyperparameters used are consistent with those in Section 6.4. We also include the Baseline column from Tables 4 and 5 for comparison. The results indicate that the balancing constraint significantly improves the accuracy of the globally optimal solution, outperforming the S3VM without this constraint in most cases. Specifically, on the **ionosphere** dataset, we observe an average improvement of 4.16%, with individual instances showing impressive accuracy gains (up to 17.98%). Additionally, for the **heart** dataset, the average accuracy without the balancing constraint falls below the baseline, whereas including the constraint raises it above the baseline.

Even when including the balancing constraint, the global minimum may not improve on the (supervised) baseline. This may happen for several reasons: an incorrect choice of hyperparameters, the clustering assumption not being verified, or the unlabeled data points not providing additional information compared to the labeled ones. Failure of the clustering assumption is our conjecture on the **connectionist** dataset, where we also tested different sets of hyperparameters, managing to improve the accuracy of the baseline only very rarely. Different is the case of the four instances discussed in the previous section, namely two instances of **arrhythmia** with 10% and 20% of labeled data points, and two instances of **musik** with 10% of labeled data points. In all four instances, the linear kernel was chosen by the cross-validation procedure.

Table 6: We report the instance name, the number of labeled data points l , the number of unlabeled data points $n - l$, the accuracy of the S3VM solution without the balancing constraint (No balancing [%]), the accuracy of the S3VM solution with the balancing constraint (Balancing [%]), the accuracy of a supervised SVM built on the labeled data points and tested on the unlabeled ones (Baseline [%]). We highlight in boldface the labeling that achieves the highest accuracy on the unlabeled data points. Additionally, we report the average accuracy for each method.

Instance	l	$n - l$	No balancing [%]	Balancing [%]	Baseline [%]
ionosphere	34	317	73.82	91.80	81.70
ionosphere	34	317	89.91	88.33	88.96
ionosphere	34	317	85.17	87.38	84.23
ionosphere	70	281	90.04	90.75	90.04
ionosphere	70	281	85.05	91.46	85.05
ionosphere	70	281	87.19	88.61	87.54
ionosphere	104	247	90.69	90.28	90.69
ionosphere	104	247	85.43	88.26	86.64
ionosphere	104	247	89.88	89.47	90.69
Average			85.23	89.36	86.31
heart	27	243	77.37	81.89	80.25
heart	27	243	80.66	80.25	79.42
heart	27	243	71.19	69.96	70.37
heart	54	216	81.94	83.33	82.41
heart	54	216	81.94	84.72	82.87
heart	54	216	76.39	76.85	75.93
heart	81	189	85.19	85.19	85.19
heart	81	189	85.71	85.19	85.19
heart	81	189	82.54	84.13	83.07
Average			80.33	81.28	80.52

We argue that the reason for the poor results was the wrong kernel choice, which impacts the lower bound quality. Indeed, we solve these four instances by imposing the RBF kernel and setting $C_l = 1$ (which is a standard value). The results are reported in Table 7, where we also include the lines from Table 5 to facilitate the comparison. It turns out that the gaps are much smaller even though we cannot close them in three hours. These results confirm the theoretical result that the quality of our bounding routine is related to the kernel choice. Note also that, apart from the first instance, the final accuracy on the unlabeled data points is higher in this new setting, both for us and for the baseline, confirming the better quality of the kernel.

To conclude the discussion on the achieved accuracy results, we calculate in Table 8 the average percentage accuracy over the three seeds reported by the S3VM (column Acc. [%]) and the baseline accuracy (column Base [%]) for all instances except **connectionist**. Furthermore, in the column “Impr [%]”, we report the difference between “Acc. [%]” and “Base [%]”, measuring the improvement (if positive) in the accuracy of the S3VM over the baseline supervised SVM. The average results confirm that the S3VM generally improves the average accuracy over the baseline supervised SVM. Increasing the number of labeled data points also enhances accuracy for both the S3VM and the baseline SVM. For some datasets, the S3VM demonstrates

Table 7: In this table, we show the performance of our solver on four problematic instances by changing the kernel. We report the instance name, the number of labeled data points l , the number of unlabeled data points $n - l$, the kernel, the penalty parameter C_l , the percentage gap (Gap [%]), the number of nodes (Nodes), the computational time in seconds (Time [s]), the accuracy of the produced solution on the unlabeled data points (Acc. [%]), the accuracy of a supervised SVM built on the labeled data points and tested on the unlabeled ones (Base [%]). We highlight in boldface the labeling that achieves the highest accuracy on the unlabeled data points.

Instance	l	$n - l$	Kernel	C_l	Gap [%]	Nodes	Time [s]	Acc. [%]	Base [%]
arrhythmia	44	408	linear	0.10	9.50	563	10800	69.12	69.61
arrhythmia	44	408	RBF	1	0.79	453	10800	68.87	66.67
arrhythmia	90	362	linear	0.32	10.91	532	10800	67.40	67.13
arrhythmia	90	362	RBF	1	0.29	435	10800	70.99	69.89
musk	46	430	linear	0.79	30.75	323	10800	70.23	69.3
musk	46	430	RBF	1	0.51	277	10800	76.51	75.81
musk	46	430	linear	0.10	9.11	503	10800	67.44	66.51
musk	46	430	RBF	1	0.49	382	10800	76.28	70.47

more significant improvements with fewer labeled data points, affirming that semi-supervised learning is particularly advantageous when labeled data is scarce. However, this increase in accuracy comes with the trade-off of significantly higher computational times, as we are solving a challenging global optimization problem.

Note that if a heuristic algorithm returns a low-quality solution, it is not possible to understand whether the solution is a bad local minimum or whether, for the given instance, the S3VM approach is not viable. On the other hand, we provide an exact method to directly establish the usefulness of the S3VM approach, at least for a given choice of hyperparameters. To the best of our knowledge, no other exact solution methods exist for real-world instances of such magnitude.

The topic of this paper reinforces the cross-fertilization between mathematical optimization and machine learning, showing that optimization can be beneficial to machine learning (and vice versa) when competencies from both worlds are put together. From the optimization perspective, we have proposed an efficient method for a challenging problem. However, the correct interpretation of the results is only possible with a deep understanding of the semi-supervised learning problem. From the machine learning point of view, without the exact solver, it is impossible to decide whether the semi-supervised approach is suitable for a given instance of the problem.

7 Conclusions

We proposed an SDP-based branch-and-cut algorithm for solving S3VM instances to global optimality. Similarly to the related literature, we considered the S3VM problem as a non-convex QCQP. Then, we applied optimality-based bound tightening to obtain box constraints. These constraints allowed us to include valid inequalities, strengthening the lower bound. For the lower bounding routine, we designed a cutting-plane algorithm. The resulting SDP relaxation yields bounds significantly stronger

Table 8: In this table, we show the average accuracy across the three seeds. We report the instance name, the number of labeled data points l , the number of unlabeled data points $n - l$, the average S3VM accuracy (Acc. [%]), and the average supervised SVM accuracy (Base [%]). Additionally, we report in the column “Impr [%]” the difference between the columns “Acc. [%]” and “Base [%]”.

Instance	l	$n - l$	Acc. [%]	Base [%]	Impr [%]
art100	10	90	93.70	92.96	0.74
art100	20	80	94.58	91.67	2.92
art100	30	70	94.76	90.00	4.76
art150	14	136	87.74	87.25	0.49
art150	29	121	88.43	87.60	0.83
art150	44	106	88.05	87.11	0.94
heart	27	243	77.37	76.68	0.69
heart	54	216	81.63	80.40	1.23
heart	81	189	84.84	84.48	0.35
2moons	30	270	92.22	92.10	0.12
2moons	60	240	99.31	99.31	0.00
2moons	90	210	99.21	99.21	0.00
ionosphere	34	317	89.17	84.96	4.21
ionosphere	70	281	90.27	87.54	2.73
ionosphere	104	247	89.34	89.34	0.00
PowerCons	36	324	96.09	94.86	1.23
PowerCons	72	288	96.99	96.64	0.35
PowerCons	108	252	98.68	99.08	-0.40
GunPoint	44	407	86.89	87.72	-0.82
GunPoint	89	362	94.57	94.47	0.09
GunPoint	134	317	93.80	94.43	-0.63
arrhythmia	44	408	71.08	65.44	5.63
arrhythmia	90	362	72.10	70.53	1.56
arrhythmia	135	317	73.92	73.82	0.11
musk	46	430	73.72	72.87	0.85
musk	94	382	80.37	80.37	0.00
musk	142	334	87.02	85.33	1.69
wdbc	56	513	95.97	95.71	0.26
wdbc	113	456	95.83	95.98	-0.14
wdbc	170	399	96.07	96.32	-0.25

than those provided by convex relaxations available in the literature. For the upper bound, instead, we proposed a two-opt local search heuristic that exploits the solution of the SDP relaxation solved at each node. Computational results underscore the efficiency of our algorithm, demonstrating its capability to address instances with ten times more data points than methods currently available in the literature. To the best of our knowledge, no other exact solution method can effectively handle real-world instances of such magnitude. Clearly, achieving exact solutions comes at the cost of significantly higher computational time compared to traditional supervised SVMs, which is expected due to the non-convex nature of the optimization problem. This research provides insights from both optimization and machine learning perspectives. Firstly,

solving large instances allows an understanding of when S3VMs are effective for a specific problem. Secondly, certified optimal solutions are valuable benchmarking tools for evaluating, enhancing, and developing heuristics and approximation methods. Such methods are fundamental in the machine learning literature. Thirdly, we assessed both theoretically and numerically the challenges that may arise when solving instances to global optimality and achieving high accuracy. The bottleneck in our algorithm lies in the lower bound computation, where we employed an off-the-shelf interior-point solver. For future research, we aim to design a tailored Alternating Direction Method of Multipliers (ADMM) algorithm capable of handling significantly larger sizes (more than a thousand data points) and a substantial number of valid inequalities. This should make the solution of the SDPs faster and more robust, leading to a more efficient branch-and-cut algorithm.

Acknowledgements

Veronica Piccialli has been supported by PNRR MUR project PE0000013-FAIR. This research was funded in part by the Austrian Science Fund (FWF) [10.55776/DOC78]. For open access purposes, the author has applied a CC BY public copyright license to any author-accepted manuscript version arising from this submission.

Statements and Declarations

Competing Interests

The authors have no relevant financial or non-financial interests to disclose.

References

- [1] Cortes, C., Vapnik, V.: Support-vector networks. *Mach. Learn.* **20**(3), 273–297 (1995) <https://doi.org/10.1007/BF00994018>
- [2] Piccialli, V., Sciandrone, M.: Nonlinear optimization and support vector machines. *4OR* **16**(2), 111–149 (2018) <https://doi.org/10.1007/s10288-018-0378-2>
- [3] Bennett, K., Demiriz, A.: Semi-supervised support vector machines. In: Kearns, M., Solla, S., Cohn, D. (eds.) *Advances in Neural Information Processing Systems*, vol. 11. MIT Press, Cambridge (1998)
- [4] Chapelle, O., Zien, A.: Semi-supervised classification by low density separation. In: Cowell, R.G., Ghahramani, Z. (eds.) *Proceedings of the Tenth International Workshop on Artificial Intelligence and Statistics. Proceedings of Machine Learning Research*, vol. R5, pp. 57–64. PMLR, Barbados (2005). Reissued by PMLR on 30 March 2021.

- [5] Chapelle, O., Scholkopf, B., Zien, A.: Semi-supervised learning (Chapelle, O. et al., eds.; 2006)[Book Reviews]. *IEEE Trans. Neural Netw.* **20**(3), 542–542 (2009) <https://doi.org/10.1109/TNN.2009.2015974>
- [6] Chapelle, O., Sindhwani, V., Keerthi, S.S.: Optimization techniques for semi-supervised support vector machines. *J. Mach. Learn. Res.* **9**(7), 203–233 (2008)
- [7] Ding, S., Zhu, Z., Zhang, X.: An overview on semi-supervised support vector machine. *Neural. Comput. Appl.* **28**(5), 969–978 (2017) <https://doi.org/10.1007/s00521-015-2113-7>
- [8] Joachims, T.: Transductive inference for text classification using support vector machines. In: *Proceedings of the Sixteenth International Conference on Machine Learning. ICML '99*, pp. 200–209. Morgan Kaufmann Publishers Inc., San Francisco, CA, USA (1999)
- [9] Burgard, J.P., Pinheiro, M.E., Schmidt, M.: Mixed-integer quadratic optimization and iterative clustering techniques for semi-supervised support vector machines. *arXiv preprint arXiv:2303.12532* (2023)
- [10] Chapelle, O., Chi, M., Zien, A.: A continuation method for semi-supervised SVMs. In: *Proceedings of the 23rd International Conference on Machine Learning. ICML '06*, pp. 185–192. Association for Computing Machinery, New York, NY, USA (2006). <https://doi.org/10.1145/1143844.1143868>
- [11] Fung, G., Mangasarian, O.L.: Semi-supervised support vector machines for unlabeled data classification. *Optim. Methods Softw.* **15**(1), 29–44 (2001) <https://doi.org/10.1080/10556780108805809>
- [12] Collobert, R., Sinz, F., Weston, J., Bottou, L.: Large scale transductive SVMs. *J. Mach. Learn. Res.* **7**, 1687–1712 (2006)
- [13] De Bie, T., Cristianini, N.: Semi-supervised learning using semi-definite programming. In: *Semi-Supervised Learning*. The MIT Press, Cambridge (2006). <https://doi.org/10.7551/mitpress/9780262033589.003.0007>
- [14] Bai, Y., Yan, X.: Conic relaxations for semi-supervised support vector machines. *J. Optim. Theory Appl.* **169**(1), 299–313 (2016) <https://doi.org/10.1007/s10957-015-0843-4>
- [15] Astorino, A., Fuduli, A.: Nonsmooth optimization techniques for semisupervised classification. *IEEE Trans. Pattern Anal. Mach. Intell.* **29**(12), 2135–2142 (2007) <https://doi.org/10.1109/TPAMI.2007.1102>
- [16] Sindhwani, V., Keerthi, S.S., Chapelle, O.: Deterministic annealing for semi-supervised kernel machines. In: *Proceedings of the 23rd International Conference*

- on Machine Learning. ICML '06, pp. 841–848. Association for Computing Machinery, New York, NY, USA (2006). <https://doi.org/10.1145/1143844.1143950>
- [17] Chapelle, O., Sindhwani, V., Keerthi, S.: Branch and bound for semi-supervised support vector machines. In: Schölkopf, B., Platt, J., Hoffman, T. (eds.) *Advances in Neural Information Processing Systems*, vol. 19. MIT Press, Cambridge (2006)
 - [18] Bai, Y., Chen, Y., Niu, B.L.: SDP relaxation for semi-supervised support vector machine. *Pacific J. Optim.* **8**, 3–14 (2012)
 - [19] Bai, Y.Q., Niu, B.L., Chen, Y.: New SDP models for protein homology detection with semi-supervised SVM. *Optimization* **62**(4), 561–572 (2013) <https://doi.org/10.1080/02331934.2011.611515>
 - [20] Wolkowicz, H., Saigal, R., Vandenberghe, L.: *Handbook of Semidefinite Programming: Theory, Algorithms, and Applications*. International Series in Operations Research & Management Science, vol. 27. Springer, New York (2012)
 - [21] Tian, Y., Luo, J.: A new branch-and-bound approach to semi-supervised support vector machine. *Soft Comput.* **21**(1), 245–254 (2017) <https://doi.org/10.1007/s00500-016-2089-y>
 - [22] Xu, L., Neufeld, J., Larson, B., Schuurmans, D.: Maximum margin clustering. In: Saul, L., Weiss, Y., Bottou, L. (eds.) *Advances in Neural Information Processing Systems*, vol. 17. MIT Press, Cambridge (2004)
 - [23] Gleixner, A.M., Berthold, T., Müller, B., Weltge, S.: Three enhancements for optimization-based bound tightening. *J. Global Optim.* **67**(4), 731–757 (2017) <https://doi.org/10.1007/s10898-016-0450-4>
 - [24] Sherali, H.D., Tuncbilek, C.H.: A reformulation-convexification approach for solving nonconvex quadratic programming problems. *J. Global Optim.* **7**(1), 1–31 (1995) <https://doi.org/10.1007/BF01100203>
 - [25] Ryoo, H.S., Sahinidis, N.V.: A branch-and-reduce approach to global optimization. *J. Global Optim.* **8**(2), 107–138 (1996) <https://doi.org/10.1007/BF00138689>
 - [26] Lubin, M., Dowson, O., Dias Garcia, J., Huchette, J., Legat, B., Vielma, J.P.: JuMP 1.0: Recent improvements to a modeling language for mathematical optimization. *Math. Program. Comput.* (2023) <https://doi.org/10.1007/s12532-023-00239-3>